Published in "The Journal of Comparative Neurology 513(6): 643 - 667, 2009"
which should be cited to refer to this work.

# A Map of Octopaminergic Neurons in the *Drosophila* Brain

SEBASTIAN BUSCH,[1,2] MAREIKE SELCHO,[1] KEI ITO,[3] AND HIROMU TANIMOTO[1,2*]
[1]Lehrstuhl für Genetik und Neurobiologie, Universität Würzburg, 97074 Würzburg, Germany
[2]Max-Planck-Institut für Neurobiologie, 82152 Martinsried, Germany
[3]Institute of Molecular and Cellular Biosciences, University of Tokyo, Yayoi, Bunkyo-ku, Tokyo 113-0032, Japan



**ABSTRACT**

**The biogenic amine octopamine modulates diverse behaviors in invertebrates. At the single neuron level, the mode of action is well understood in the peripheral nervous system owing to its simple structure and accessibility. For elucidating the role of individual octopaminergic neurons in the modulation of complex behaviors, a detailed analysis of the connectivity in the central nervous system is required. Here we present a comprehensive anatomical map of candidate octopaminergic neurons in the adult *Drosophila* brain: including the supra- and subesophageal ganglia. Application of the Flp-out technique enabled visualization of 27 types of individual octopaminergic neurons. Based on their morphology and distribution of genetic markers, we found that most octopaminergic neurons project to multiple brain structures with a clear separation of dendritic and presynaptic regions. Whereas their major dendrites are confined to specific brain regions, each cell type targets different, yet defined, neuropils distributed throughout the central nervous system. This would allow them to constitute combinatorial modules assigned to the modulation of distinct neuronal processes. The map may provide an anatomical framework for the functional constitution of the octopaminergic system. It also serves as a model for the single-cell organization of a particular neurotransmitter in the brain.**

The biogenic amine octopamine (OA), analogous to the vertebrate noradrenaline, acts as a neurohormone, neuromodulator, and neurotransmitter in invertebrates. Owing to the simple architecture and accessibility, the insect peripheral nervous system is well suited for studying the neuronal circuits underlying the diverse functions of OA (Roeder, 1999, 2005; Farooqui, 2007). For instance, OA release from a single thoracic dorsal unpaired median (DUM) neuron modulates synaptic potential and tension of the extensor tibiae muscle in the locust (Evans and O'Shea, 1977). OA synthesis in a subset of abdominal octopaminergic neurons innervating the oviduct muscle was sufficient to restore a severe defect in ovulation in a *Drosophila* mutant lacking OA (Monastirioti et al., 1996; Monastirioti, 2003). Similarly, stimulation of the octopaminergic neuron innervating the corpora cardiaca in the locust was shown to liberate the adipokinetic hormones into the hemolymph (Downer et al., 1984). Specific mesothoracic DUM neurons were proposed to enhance the response of the forewing stretch receptor during flight by releasing OA into the hemolymph (Ramirez and Orchard, 1990).

Genetic, pharmacological, and electrophysiological studies have revealed that OA in the central nervous system (CNS) controls more complex behaviors and general internal states, such as aggression and stress resistance (Mercer and Menzel, 1982; Adamo et al., 1995; Scholz et al., 2000; Stevenson et al., 2000; Schwaerzel et al., 2003; Schroll et al., 2006; Vergoz et al., 2007; Certel et al., 2007; Hoyer et al., 2008). In olfactory learning the octopaminergic system is selectively required for reward processing, but not for odor perception or general learning ability (Schwaerzel et al., 2003; Schroll et al., 2006; Vergoz et al., 2007). Similarly, the *Drosophila* mutant lacking OA cannot develop normal ethanol tolerance, while the ethanol sensitivity remains intact (Scholz et al., 2000). However, due to their complex structure and limited accessibility, there

Grant sponsor: Emmy-Noether Program from Deutsche Forschungsgemeinschaft (to H.T.); Grant sponsor: Max-Planck-Gesellschaft (to H.T.); Grant sponsor: Institute for Bioinformatics Research, Development/Japan Science and Technology Agency (BIRD/JST; to K.I.); Grant sponsor: Grant-in-Aid for Scientific Research from the Ministry of Education, Culture, Sports, Science and Technology of Japan (to K.I.).

Present address for M. Selcho: Department of Biology, University of Fribourg, Chemin du Musée 10, 1700 Fribourg, Switzerland.

*Correspondence to: Hiromu Tanimoto, Max-Planck-Institut für Neurobiologie, Am Klopferspitz 18, 82152 Martinsried, Germany.
E-mail: hiromut@neuro.mpg.de

are few studies on the architecture and behavioral function of individual octopaminergic neurons in the CNS (e.g., Certel et al., 2007; Zhou and Rao, 2008). A notable exception is VUMmx1, one of the ventral unpaired median (VUM) neurons, in the honeybee. Electrical stimulation of VUMmx1 could substitute the sugar reward in associative olfactory learning (Hammer, 1993). Another example is the locust PM4 neurons, which innervate the optic lobe. They contribute to the dishabituation of the visual interneuron DCMD presumably by releasing OA (Stern, 1999). To systematically understand the function of each octopaminergic neuron, a comprehensive anatomical description is essential.

Comparative anatomical studies of such neurons revealed striking similarities among different insect species (Konings et al., 1988; Spörhase-Eichmann et al., 1992; Kreissl et al., 1994; Stern et al., 1995; Monastirioti et al., 1995; Dacks et al., 2005; Sinakevitch et al., 2005; Sinakevitch and Strausfeld, 2006). In all insects analyzed a small number of octopaminergic neurons as a group profusely ramify in most, if not all, neuropil structures of the brain. Each cluster of somata contributes to a distinct system of arborizations (Sinakevitch et al., 2005; Sinakevitch and Strausfeld, 2006)

In the locust and the honeybee a specific class of putative octopaminergic neurons in the subesophageal ganglion (SOG) was reconstructed at single-cell resolution utilizing intracellular staining (Bräunig, 1991; Schröter et al., 2007). The DUM neurons in *Locusta migratoria* and VUM neurons in *Apis mellifera* are unpaired and exhibit bilaterally symmetric innervations. Their cell bodies are located along the dorsal and ventral midline, respectively. The locust DUM and honeybee VUM neurons in the SOG comprise cells descending to the thoracic ganglia via the cervical connectives as well as ascending neurons that innervate principal brain neuropils such as the mushroom bodies, the antennal lobes, and the central complex (Bräunig, 1991; Bräunig and Burrows, 2004; Schröter et al., 2007). Since the number and localization of the midline neurons correlate with OA cytochemistry, all the DUM and VUM neurons analyzed in these studies are supposed to be octopaminergic (Bräunig, 1991; Kreissl et al., 1994; Sinakevitch et al., 2005; Schröter et al., 2007).

In *Drosophila* there are 100 octopaminegic neurons in the brain (Sinakevitch and Strausfeld, 2006). However, their complex and dense ramifications made it difficult to analyze the morphology of single neurons. Hence, the innervation and connectivity patterns of individual neurons are hitherto poorly understood. As a first step toward the cellular basis of OA-mediated neuromodulation and diverse behaviors, we analyzed the morphology of single octopaminergic neurons in the adult *Drosophila* brain. By applying the Flp-out technique (Wong et al., 2002) to GAL4 lines labeling octopaminergic neurons, here we systematically identify the morphology of individual neurons in the SOG and the brain. These neurons constitute the anatomical framework of the system that should mediate the modulatory functions of OA.

## MATERIALS AND METHODS

### Flies and genetic crosses

Flies were cultured on standard *Drosophila* medium (semolina, agar, molasses, yeast, nipagin) under a constant light/dark cycle (14/10 hours) at 25°C. *tdc2-GAL4* [II] (Cole et al., 2005) and the enhancer trap line *NP7088* [II] (Hayashi et al., 2002) were examined as driver lines to label specific subsets of octopaminergic neurons. *NP7088* was identified through a large-scale database screening for mushroom body extrinsic neurons (Tanaka et al., 2008). Employed reporter genes were *UAS-mCD8::GFP* [X] (Lee and Luo, 1999), *UAS-Rdl-HA* [X; III] (Sanchez-Soriano et al., 2005), and *UAS-Syt-HA* [X] (Robinson et al., 2002).

To examine GAL4-positive neurons, strains carrying either of the GAL4 drivers and *UAS-mCD8::GFP* were generated. These lines were utilized to analyze the innervation pattern as well as the colocalization with OA-immunoreactivity. To map pre- or postsynaptic regions simultaneously with GAL4-expressing neurons, the flies with the following genotypes were generated: *y w UAS-mCD8::GFP/UAS-Rdl-HA; tdc2-GAL4/+; UAS-Rdl-HA/+* and *y w UAS-mCD8::GFP/y w UAS-Syt-HA; tdc2-GAL4/+;syn$^{97}$/+*.

For single-cell analyses, females of *y w hsp70-flp* [X]; *UAS>CD2 y$^{+}$>mCD8::GFP/CyO* [II]*; TM2/TM6b* (Wong et al., 2002) were crossed to males of each GAL4 strain. Crosses were raised at 18°C and the parental generations were transferred to new vials every 2 days for synchronized development. To remove the Flp out cassette (*CD2 y$^{+}$*), animals received a heat shock between 3 and 13 days after egg laying at 37°C for 20–30 minutes. *Cy$^{+}$* female progeny from these crosses were selected for the single-cell analysis.

### Immunhistochemistry

***Standard staining for whole mounts.*** The brains were dissected by removing cuticles and connective tissues and immediately fixed for 2 hours at room temperature in 4% formaldehyde in phosphate-buffered saline (PBS, pH 7,4) containing 0.3% Triton X-100 (PBT; Sigma, St. Louis, MO). Subsequently, the samples were rinsed three times with PBT and blocked with 3% normal goat serum (Jackson ImmunoResearch, West Grove, PA) in PBT. The brains were incubated with the primary antibodies in blocking solution at 4°C overnight. Samples were washed six times with PBT and incubated with secondary antibodies in the blocking solution overnight at 4°C. After washing the brains six times with PBT they were mounted in Vectashield (Vector, Burlingame, CA).

***Octopamine and tyramine staining.*** For immunostaining of OA and tyramine (TA), we used a modified version of the staining protocol of Sinakevitch and Strausfeld (2006). The 4–5-day-old flies were paralyzed on ice. The head capsule was opened in fixative containing 0.65% glutaraldehyde in 0.1 M sodium cacodylate buffer (pH 7.5) with 1% sodium metabisulfate (SMB; Sigma) and prefixed for 5 minutes on ice. The brains were removed in fixative and subsequently fixed for 2 hours at room temperature. After washing the specimens four times with 0.05 M Tris-HCl containing 0.45% SMB (Tris-HCl SMB, pH 7.4), they were treated with 0.3% sodium borohydride (Sigma) in Tris-HCl SMB. The brains were rinsed four times with Tris-HCl SMB and two times with Tris-HCl SMB containing 0.5% Triton-X 100 (Tris-HCl SMB TX, pH7.5; TX, Sigma). Samples were blocked for 1.5 hours with 10% normal goat serum in Tris-HCl SMB TX and incubated with the primary antibodies in blocking solution at 4°C for 48 hours. Subsequently specimens were rinsed five times with Tris-HCl TX before incubation with secondary antibodies in blocking solution at 4°C overnight. The brains were washed five times

TABLE 1. Utilized Primary Antibodies

| Antigen | Immunogen | Manufacturer, species, type, catalog number | Dilution used |
|---|---|---|---|
| Octopamine (OA) | Octopamine coupled to thyroglobulin by means of glutaraldehyde | Jena Bioscience (Jena, Germany), mouse monoclonal, #ABD-029 | 1:1,000 |
| p-Tyramine (TA) | p-Tyramine conjugated to BSA by glutaraldehyde | Chemicon International (Temecula, CA), rabbit polyclonal, #AB124 | 1:200 |
| Green fluorescent protein (GFP) | GFP isolated from *Aequorea victoria* | Invitrogen (Eugene, OR), rabbit polyclonal, #A6455 | 1:5,000 |
| *Influenza* hemagglutinin epitope (YPYDVPDYA) | Synthetic peptide, CYPYDVPDYASL | Covance (Berkeley, CA), mouse monoclonal, clone 16B12, #MMS-101P | 1:1,000 |
| *Drosophila* Synapsin | First open reading frame of the *Drosophila* Synapsin protein | Klagges et al., mouse monoclonal | 1:20 |

with Tris-HCl TX and twice in Tris-HCl. Subsequently they were mounted in Vectashield (Vector).

## Primary antibodies

Information of employed primary antibodies and experimental conditions are summarized in Table 1.

The specificity of the monoclonal anti-OA antibody was examined with an indirect competitive enzyme-linked immunosorbent assay (ELISA) and revealed that it has high affinity to the tested OA-poly-L-lysine conjugate (Dacks et al., 2005). Relative crossreactivity was detected for epinephrine, norepinephrine, and TA, but not for dopamine, DOPA, or serotonin (Dacks et al., 2005). To further verify the specificity of the anti-OA antibody, we immunostained the wildtype *Drosophila* brain with the primary antibody solution after preincubating it for 2 hours at 4°C with 250 $\mu$g/mL OA-conjugated bovine serum albumin (BSA). This treatment abolished the labeling of somata and fibers in the brain, in contrast to the control treatment with BSA alone (Suppl. Fig. 2). In both groups, however, we found strong and ubiquitous background staining, particularly in the cortical regions. This may be due to unspecific binding of the primary antibody to the glutaraldehyde-fixed tissue, given less background by omitting the primary antibody (Suppl. Fig. 2G,H). To evaluate the crossreactivity to TA in the fly brain, we carried out double immunolabeling using the anti-OA and anti-TA antibodies (Suppl. Fig. 3). All OA-positive cells were also colabeled by the anti-TA antibody. Some cell bodies were strongly labeled by the anti-TA, but not by the anti-OA antibody. This suggests that the crossreactivity of the anti-OA antibody to TA is negligible in practice.

The specificity of the anti-TA antibody was tested by an equilibrium dialysis using radiolabeled TA conjugated to N-$\alpha$-acetyl-L-lysine N-methylamide (ALM; Geffard et al., 1984). Competition experiments were performed with the labeled ligand and several unlabeled catecholamine conjugates including TA-ALM. Subsequently the crossreactivity-ratio at half displacement was determined. TA-ALM turned out to induce the best displacement (crossreactivity ratio = 1). Octopamine-ALM was 42 times less immunoreactive than TA-ALM; L-DOPA by a factor of 100. Dopamine-ALM and noradrenaline-ALM showed no displacement (Geffard et al., 1984).

We verified that the anti-GFP and anti-HA antibodies do not crossreact with endogenous molecules in the wildtype *Drosophila* brain (see Suppl. Fig. 1). The signal is specifically detected after expressing the respective transgenic epitopes encoded by the effector genes (compare Figs. 1, 4, 5, and Suppl. Fig. 1). We used two different HA-tagged reporter-genes, Syt-HA and Rdl-HA, respectively. Driven with *tdc2-GAL4*, Rdl-HA and Syt-HA show distinct subcellular localizations. This indicates that anti-HA specifically detects the HA-tag rather than the fused marker proteins.

GAL4-independent expression of the effector genes was verified with the reporter strains in the absence of a GAL4 driver (Suppl. Fig. 1). There was leaky expression in *UAS-syt-HA* with a specific pattern (Suppl. Fig. 1), although it was much less than the signals in the presence of the GAL4.

The monoclonal anti-Synapsin antibody was previously shown to recognize multiple Synapsin isoforms on Western blots with wildtype heads, which disappeared in the deletion mutant (Klagges et al., 1996; Godenschwege et al., 2004). Consistently, the antibody did not give a signal to cryosections of the *synapsin* mutant brain, although it clearly stained the synaptic neuropils in the wildtype fly (Klagges et al., 1996; Godenschwege et al., 2004). Utilizing anti-Synapsin we obtained a characteristic staining pattern in the *Drosophila* brain that is identical with previous reports (Godenschwege et al., 2004).

The specificity of the anti-HA antibody was additionally verified in Western blot, where a single band at 46 kD, corresponding to the HA-tagged protein Stm1p, was detected specifically upon transgenic expression (van Dyke et al., 2004).

## Secondary antibodies

Alexa Fluor 488 conjugated goat anti-rabbit IgG (1:2,000, Molecular Probes, Eugene, OR; A11034) and Cy3 conjugated goat anti-mouse IgG (1:500 [1:250 to detect the anti-OA antibody], Jackson ImmunoResearch; 115-166-003) were used to detect primary antibodies.

## Microscopy and image editing

Samples were scanned at confocal microscopes (Leica SP1, SP2, or SP5). A stack of images was collected at 1 or 1.5 $\mu$m steps with a 40× or a 20× objective, respectively. Projections and selections of the confocal stacks were accomplished with ImageJ (NIH, Bethesda, MD). Brightness, contrast as well as the color of each channel was adjusted with Adobe Photoshop 7.0 (San Jose, CA). To effectively visualize faint processes of the labeled neurons, stained fibers and counterstaining in most figures were presented in white (RGB ratio; 255:255:255) and orange (255:85:0), respectively.

## Nomenclature of candidate octopaminergic neurons

The *Drosophila* brain atlas of Otsuna and Ito (2006) and the corresponding terminology were used as an orientation to describe the anatomy of GAL4-positive neurons (Otsuna and

Ito, 2006). In this report we use the term "brain" collectively for the supra and subesophageal ganglia.

To name candidate octopaminergic neurons in a systematic manner without causing interference with the names of other neurons, we employed a hierarchical naming scheme. First, cell clusters are named according to their neighboring neuropils. A common prefix "OA-" was added to each cell type in order to distinguish these neurons from others in a similar location. Cells with different morphological categories in the same cluster were distinguished with an abbreviation of their characteristic projection patterns, e.g., i, b, a, and d for ipsilateral, bilateral, ascending, and descending, respectively. Finally, different cell types in each category were distinguished by adding serial numbers.

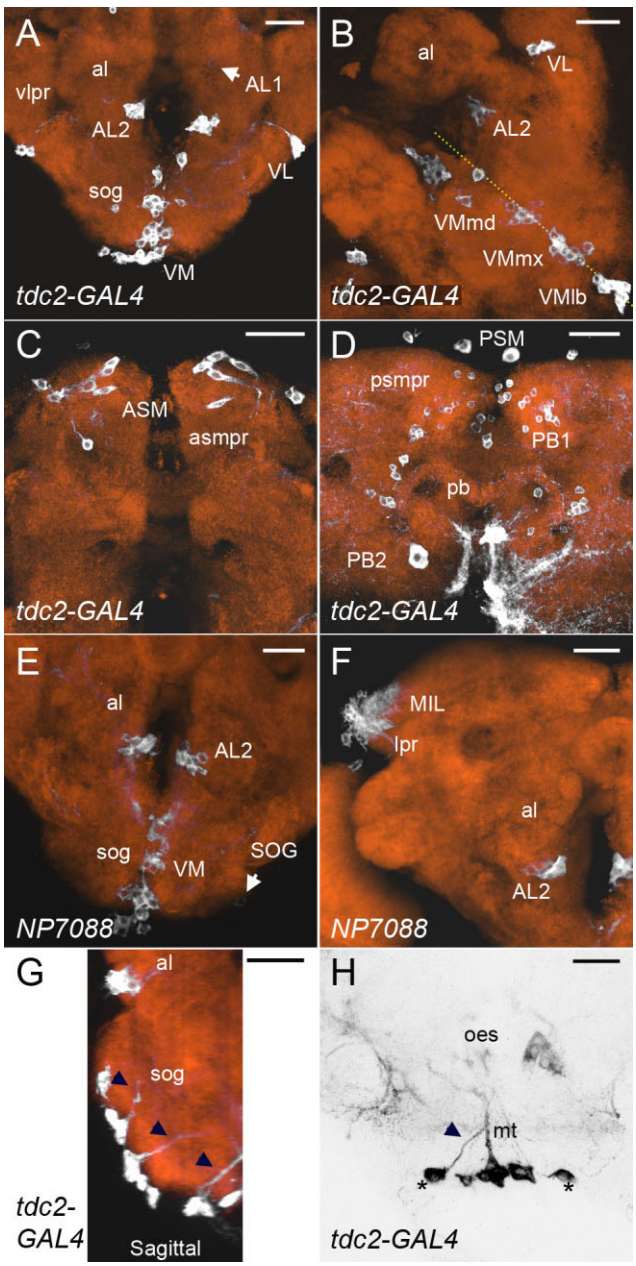


## RESULTS

### Cell clusters in the brain labeled by *tdc2-GAL4* and *NP7088*

To investigate the morphology of individual octopaminergic neurons we employed two GAL4 driver lines: *tdc2-GAL4* (Cole et al., 2005) and *NP7088* (Tanaka et al., 2008). *tdc2-GAL4* is a GAL4 driver under the control of a regulatory sequence of the tyrosine decarboxylase gene (*tdc*) (Cole et al., 2005). Since *tdc2* encodes an enzyme catalyzing the synthesis of TA, the precursor of OA, octopaminergic neurons express Tdc2. The GAL4 enhancer trap line *NP7088* was isolated in the anatomical screen of the NP strains (Hayashi et al., 2002) for the extrinsic neurons of the mushroom body (Tanaka et al., 2008). Since some of the tracts and terminal arborizations in *NP7088* resemble the distribution of OA immunoreactivity (Sinakevitch and Strausfeld, 2006; Tanaka et al., 2008), we decided to investigate this strain as well as *tdc2-GAL4*. We first describe the position of the GAL4-positive cell clusters in each line, and subsequently examine which of the labeled clusters are OA-immunoreactive.

To determine the positions of the cell bodies in *tdc2-GAL4* and *NP7088*, we expressed mCD8::GFP, a marker selectively localized to the plasma membrane. Thus, the nuclei of GAL4-expressing cells lack the transgenic label (Fig. 1). We counted 137 cells in *tdc2-GAL4* and 333 in *NP7088* on average (Table 2), although whole-mount preparation might have obscured the precise numbers of the labeled cells.

Figure 1.
GAL4 expression pattern of *tdc2-GAL4* (A–D) and *NP7088* (E,F) in the adult brain. Each panel shows a projection of confocal stacks illustrating different parts of the central brain. Neuropils and the somata of GAL4-expressing cells are visualized by $\alpha$-Synapsin (orange) and *UAS-mCD8::GFP* (white), respectively. Throughout the figures, brain regions and cell clusters are labeled with lower case and capital letters, respectively. **A:** Frontal view of the ventral SPG and SOG of *tdc2-GAL4* driving mCD8::GFP expression. The VM cluster is located along the ventral midline of the SOG (labeled sog). Cluster AL1 consists of one paired soma (arrow) at the anterior margin of the antennal lobe (al). Cluster AL2 is located ventromedial of the antennal lobe and cluster VL between the antennal lobe and the ventrolateral protocerebrum (vlpr). **B:** Oblique view from the ventral so as to better visualize the bottom of the SOG. The brain is tilted about 45° to the left; the dashed line indicates the midline of the SOG. The VM cluster is divided into three subclusters: VMmd, VMmx, and VMlb from anterior to posterior. **C:** Paired somata at the anterior superior medial protocerebrum (asmpr) constitute cluster ASM. **D:** In the posterior cortex, neurons in cluster PSM are labeled by *tdc2-GAL4* around the protocerebral bridge (pb) and at the posterior superior medial protocerebrum (psmpr). Small somata (PB1) are scattered around the protocerebral bridge. Two large somata (PB2) are located ventral to the bridge. **E:** In *NP7088*, cluster VM and AL2 are also located along the ventral midline of the SOG (sog) and ventromedial to the antennal lobes (al), respectively. Scattered and weakly labeled somata lateral to the SOG (arrow) are covered by *NP7088*, but not by *tdc2-GAL4*. **F:** Cells in cluster MIL beneath the entire lateral protocerebrum (lpr) are labeled in *NP7088*. **G:** Reconstructed sagittal projection of the confocal stacks visualizes the organization of the VM cluster in *tdc2-GAL4* along the anteroposterior axis. Neuronal processes and neuropil are visualized with *UAS-mCD8::GFP* (white) and Synapsin (orange), respectively. Each subcluster of the ventral midline (VMmd, VMmx, and VMlb from anterior [left]) sends a bundle of axons through a distinct median tract (arrowheads). **H:** Frontal projection of the VM cluster in *tdc2-GAL4*. Paired somata of the VM cluster are located slightly lateral from the midline (asterisks) with their primary neurites apart from the median tracts (arrowhead). Scale bars = 25 $\mu$m.

TABLE 2. Number of GAL4-Positive Neurons and Octopamine-Immunoreactive Population in Clusters of Cells in *tdc2-GAL4* and *NP7088*

| | *tdc2-GAL4* | | | | *NP7088* | | | |
|---|---|---|---|---|---|---|---|---|
| Cell cluster | Total cell number (SEM) | n | OA positive cells (in percent) | n | Total cell number (SEM) | n | OA-positive cells (in percent) | n |
| VM | 27 (0.65) | 8 | 78–100 | 7 | 34 (0.56) | 14 | 55–93 | 7 |
| AL2 | 7 (0.26) | 8 | 100 | 6 | 11 (0.29) | 14 | 70–100 | 7 |
| VL | 2 (0.16) | 8 | 100 | 6 | | | | |
| ASM | 8 (0.46) | 8 | 25–100 | 7 | | | | |
| AL1 | 1 (0.13) | 8 | | | | | | |
| PSM | 5 (0.62) | 8 | | | | | | |
| PB1 | 65 (3.96) | 8 | | | | | | |
| PB2 | 2 (0.13) | 8 | | | | | | |
| MIL | | | | | 97 (2.87) | 6 | | |
| PL | | | | | 19 (3.00) | 7 | | |
| MSM | | | | | 12 (3.75) | 6 | | |
| SOG | | | | | 18 (0.98) | 13 | | |
| Total (both hemispheres) | 137 (4.7) | 8 | | | 333 (13.8) | 6 | | |

The GFP-expressing cells form characteristic clusters (Fig. 1). Two major clusters appear to be commonly labeled in both lines: VM and AL2 (Fig. 1A,B,E). The VM cluster neurons have their cell bodies along the ventral midline of the SOG (Fig. 1A,B,E,G,H). Altogether, the VM cluster contains on average 27 cells in *tdc2-GAL4* and 34 in *NP7088* (Table 2). They can be divided into three subclusters along the anteroposterior axis, arguably representing three neuromeres (mandibular, maxillary, and labial) in the gnathal segment. Therefore, these subclusters are named VMmd, VMmx, and VMlb from anterior to posterior (Fig. 1B,G). Their primary tracts are distinct along the anteroposterior axis (Fig. 1G), while the cell bodies of these subclusters are not always separated clearly. Each subcluster sends an axon bundle into a corresponding median tract targeting the ventral esophagus foramen (Fig. 1G,H). These subclusters appear to differ in the numbers of constituent cells, and contain paired somata whose primary neurites run apart from the median tracts (Fig. 1H).

Cluster AL2 is located at the ventromedial margin of the antennal lobes in the supraesophageal ganglion (SPG). *tdc2-GAL4* labeled seven somata in each hemisphere (Fig. 1A,B,E, Table 2), whereas 11 neurons per hemisphere were labeled in *NP7088* (Table 2).

Several cell clusters are uniquely labeled by either of the GAL4 drivers. *tdc2-GAL4* exhibits two paired cell bodies located between the antennal lobe and the ventrolateral protocerebrum, which constitute cluster VL (Fig. 1A,B, Table 2). Cluster ASM comprises eight discrete cell bodies per hemisphere on the anterior superior medial protocerebrum (Fig. 1C, Table 2). In addition, *tdc2-GAL4* labels cells around the protocerebral bridge (PB1; 65 cells; Fig. 1D, Table 2), ventral to the protocerebral bridge (PB2; 2 cells; Fig. 1D, Table 2), on the posterior superior medial protocerebrum (PSM; 5 cells; Fig. 1D, Table 2), and at the anterior margin of the antennal lobe (AL1; 1 cell; Fig. 1A, Table 2).

In *NP7088*, additional cells are labeled in the lateral SOG (SOG; 18 cells; Fig. 1E, Table 2, Suppl. Fig. 3). There are three additional distinguishable cell clusters in the lateral or dorsal cortex: clusters MIL, MSM, and PL on the middle inferior lateral, the middle superior medial, and the posterior lateral protocerebra, respectively (97, 12, or 19 cells, respectively; Table 2, Fig. 1F, Suppl. Fig. 3).

## Octopamine immunoreactivity

Some of the GFP-labeled clusters (VM, AL2, VL, and PB1) have their cell bodies in the brain regions where OA-immunoreactive cell clusters have been reported (Monastirioti et al., 1995; Sinakevitch and Strausfeld, 2006). To clarify which of the GFP-positive clusters are OA-immunoreactive, we labeled brains expressing mCD8::GFP under the control of *tdc2-GAL4* or *NP7088* with the monoclonal anti-OA antibody (Dacks et al., 2005). Given the reported crossreactivity to TA, the precursor of OA (Dacks et al., 2005), it is still possible that some of the labeled clusters are tyraminergic without producing OA. Yet since the same cell clusters described here are also labeled by another polyclonal antibody, likely with different crossreactivity (Sinakevitch et al., 1995; Sinakevitch and Strausfeld, 2006) (data not shown), we collectively regard them as octopaminergic.

In *tdc2-GAL4* we detected colocalized signals in the cell bodies and thick neurites of clusters VM, AL2, VL, and ASM (Fig. 2A–H). In *NP7088*, colocalization was restricted to clusters VM and AL2 (Fig. 2I–L). In general, we observed a significant variation in the staining between specimens.

In the VM cluster of both GAL4 lines, all OA-immunoreactive cell bodies are colabeled with mCD8::GFP. This suggests that *tdc2-GAL4* and *NP7088* cover all OA-immunoreactive neurons in this region. On the other hand, there are some GFP-positive cell bodies without OA-signal (arrowheads in Fig. 2E,K), implying that not all GFP-expressing cells are octopaminergic. However, in this cluster the number of OA-immunoreactive neurons varied significantly between specimens. In the case of *tdc2-GAL4* between 78–100% of the GAL4-expressing cells were colabeled (Table 2). Considering this variation and the difficulties of OA-immunolabeling, we assume that in this line nearly all VM cluster neurons expressing GAL4 are OA-immunoreactive. In contrast, we never observed a complete overlap in *NP7088*, indicating that not all the neurons of the VM cluster labeled in this line are octopaminergic (Table 2).

Similarly, *NP7088* covers all OA-immunoreactive neurons in cluster AL2. Around 2–4 neurons per hemisphere show no OA-immunoreactivity (Fig. 2L, Table 2). With *tdc2-GAL4* the situation is different: while all GFP-expressing cells show OA-immunoreactivity, one cell body per hemisphere is OA-immunoreactive without expressing detectable GFP (arrowhead in Fig. 2F; Table 2).

Cluster VL and ASM are uniquely labeled by *tdc2-GAL4*. Both cells in cluster VL are OA-immunoreactive and vice versa (Fig. 2H, Table 2). In cluster ASM a clear determination of the number of OA-immunoreactive neurons turned out to be difficult due to the variability in OA-immunolabeling. We found

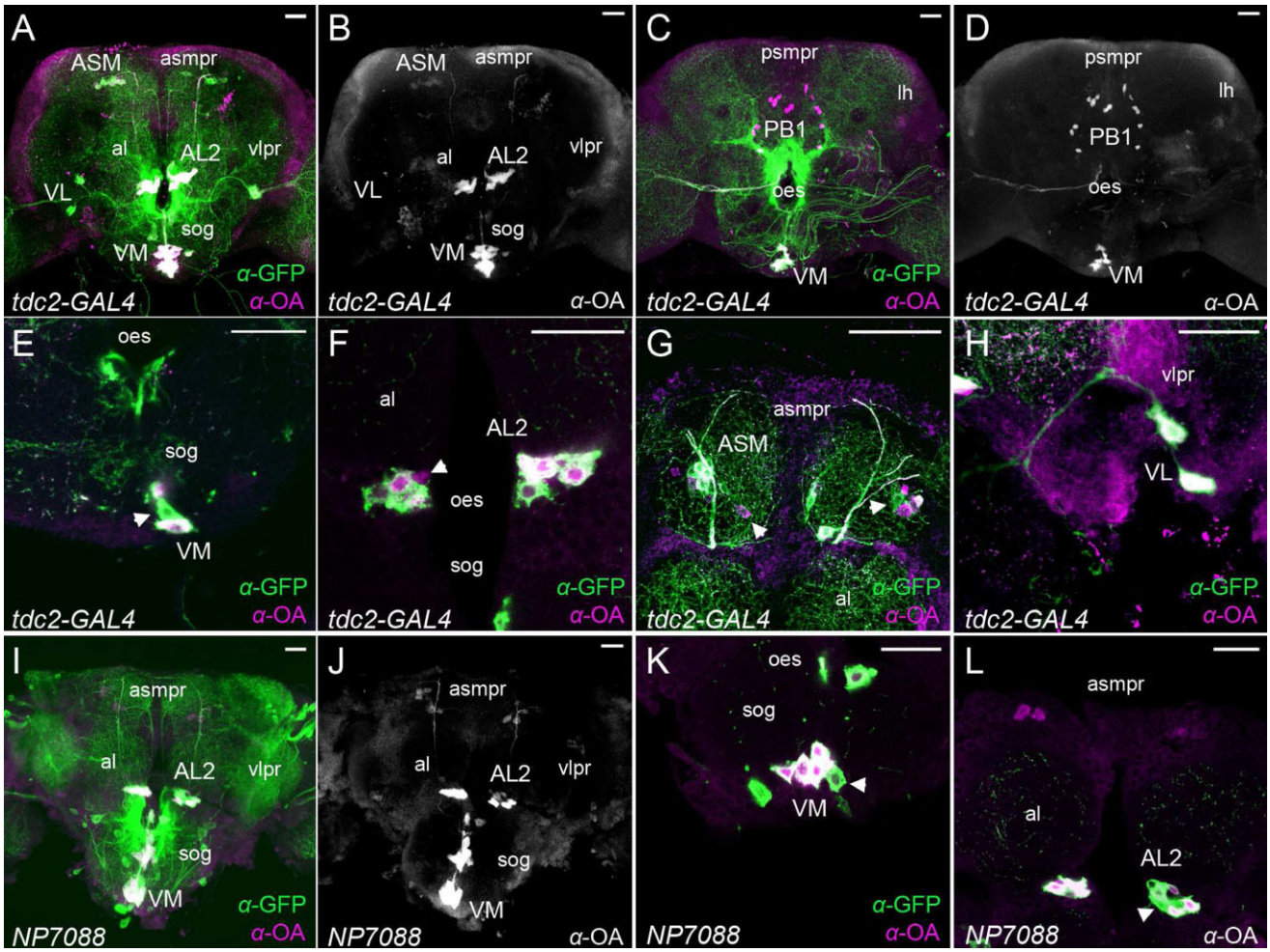


Figure 2.
OA-immunoreactivity in *tdc2-GAL4* (A–H) and *NP7088* (I–L) shown in projections of stacks (A–D,G–J) or single optical sections (E,F,K,L). OA-signal was monitored with the anti-OA antibody (α-OA; magenta). The membrane marker *UAS-mCD8::GFP* (green) labels the processes of GAL4–expressing neurons including somata. **A–D:** Confocal projections of the central brain. OA immunoreactivity in A and C is separately presented in a gray scale (B,D, respectively). The OA-signal overlaps with cluster VM, AL2, VL, and ASM in *tdc2-GAL4*. There is no detectable overlap of GFP and OA-signal in cluster PB1 (C,D). **E–H:** Magnifications of cell bodies. E: Magnification of the VM cluster. Occasionally a small population of GFP-positive neurons is labeled only faintly by α-OA given the variable staining of OA (arrowhead). F: Magnification of GFP-labeled neurons of cluster AL2 overlapping with OA-immunoreactivity. One OA-immunoreactive neuron does not overlap with GFP-signal (arrowhead). G: Several neurons in cluster ASM overlap with OA-signal. In addition, there are somata exclusively labeled by α-OA or α-GFP (arrowheads). H: GFP- and OA-signal colocalize in both cell bodies of cluster VL. **I,J:** OA-signal was colocalized in cluster VM and AL2 in *NP7088*. **K:** In cluster VM, all OA-immunoreactive somata overlap with GFP signal. Additionally, there are GFP-positive neurons not labeled with α-OA (arrowhead). **L:** OA-immunoreactive neurons of cluster AL2 colocalize with GFP-signal. However, there are several somata exclusively labeled with α-GFP (arrowhead). Scale bars = 25 μm.

several specimens that exhibit a complete overlap between GFP- and OA-labeled cells in this cluster. However, in other specimens some cells were labeled exclusively with either GFP or OA (Fig. 2G, Table 2). We therefore assume that *tdc2-GAL4* is likely to cover a subpopulation, but not all, of OA-immunoreactive neurons in cluster ASM.

The anti-OA antibody failed to label two major cell clusters in *tdc2-GAL4* and *NP7088*. Close to cluster PB1 we observed many OA-immunoreactive cell bodies, but these neurons did not appear to overlap with the GAL4 expression in *tdc2-GAL4* (Fig. 2C,D). Similarly, the ellipsoid body of the central complex is innervated by OA-immunoreactive processes (Sinakevitch and Strausfeld, 2006) (data not shown), but GFP signal was not detectable in either of the GAL4 drivers (Figs. 1, 3K). Sinakevitch and Strausfeld (2006) identified more octopaminergic cell clusters that are not GAL4-positive. These clusters were not visualized in our OA-staining and comprised a small number of cells.

## *tdc2-GAL4* and *NP7088* overlap in clusters VM and AL2

Since the majority of cells in cluster VM and AL2 are OA-immunoreactive in both lines, we assume that they label identical cells in these regions. To reveal the extent of overlap in GAL4 expression, we counted the number of the labeled cells in the brains carrying both *NP7088* and *tdc2-GAL4*. Since

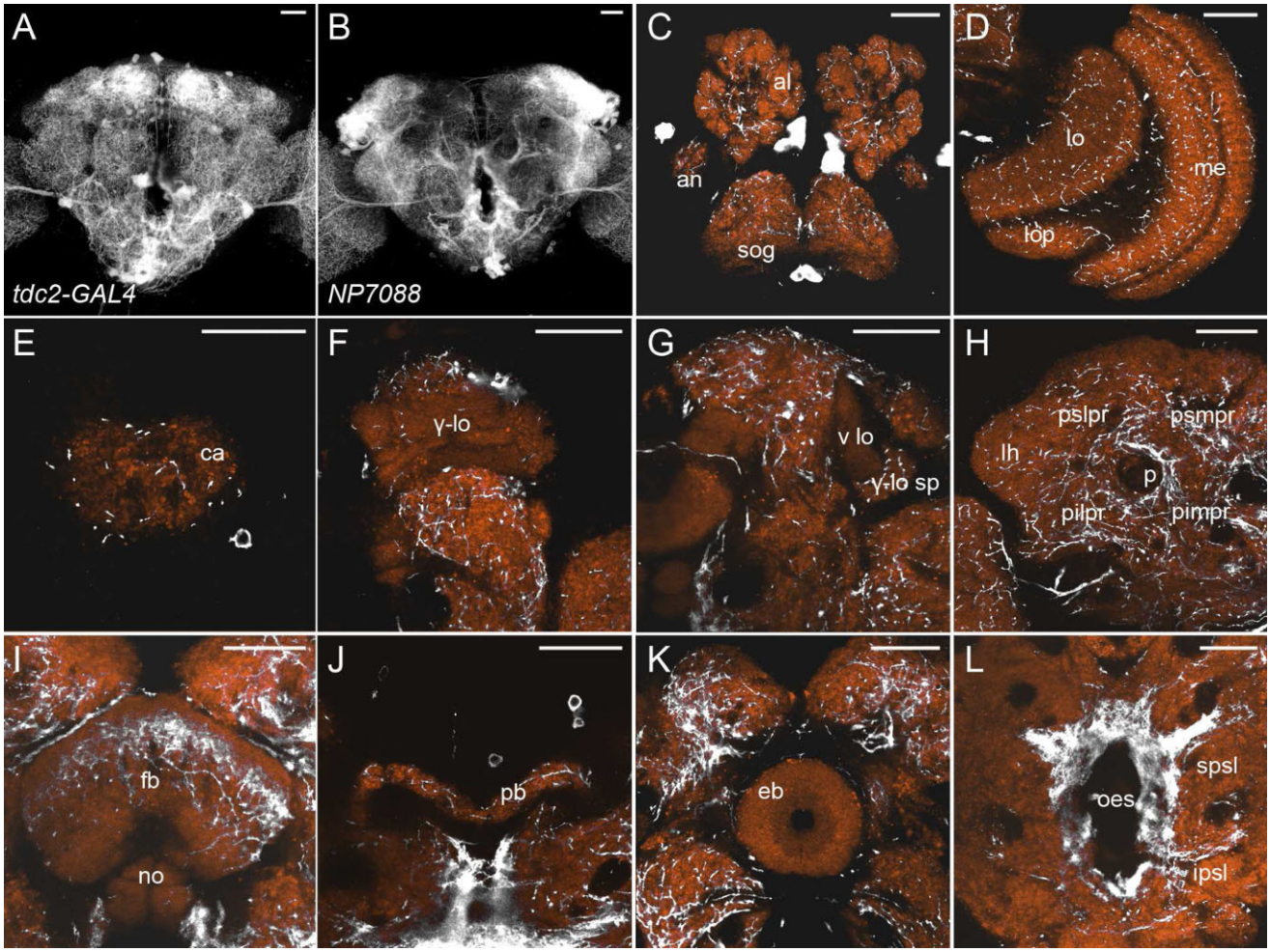


Figure 3.
Innervation pattern of GAL4-expressing neurons in the adult brain. **A,B:** Projections of confocal stacks of the central brain. *UAS-mCD8::GFP* monitors neuronal processes. Neurons labeled in *tdc2-GAL4* and *NP7088* innervate throughout the central brain. The projection pattern of both lines coincides to a large extent. **C–L:** Single confocal sections of distinct brain regions of *tdc2-GAL4*. Neuropil was visualized with the antibody against the presynaptic vesicle protein Synapsin (orange). C: Fine neuronal processes are found throughout the antennal lobes (al), antennal nerves (an) and SOG (sog). D: The lobula (lo), lobula plate (lop) and medulla (me) in the optic lobes are innervated by these neurons. E–H: In the mushroom body, neuronal processes innervate the entire calyx (ca), the γ-lobe (γ-lo), and the spur of the γ-lobe (γ-lo sp). Neither the remaining parts of the lobes (vertical lobes, vlo) nor the pedunculus (p) of the mushroom body is labeled in both GAL4 lines. The GFP-positive innervation is detected throughout the protocerebrum such as the lateral horn (lh), posterior superior lateral protocerebrum (pslpr); posterior superior medial protocerebrum (psmpr); posterior inferior lateral protocerebrum (pilpr) and posterior inferior medial protocerebrum (pimpr). I–K: In the central complex the fan-shaped body (fb), the nodulli (no), and the protocerebral bridge (pb) are innervated. Despite the presence of OA signal, the ellipsoid body (eb) is not innervated by the GAL4-expressing cells in both lines. L: Conspicuously dense ramifications spread in the superior (spsl) and inferior posterior slope (ipsl) surrounding the esophagus (oes) foramen. Along the anterior/posterior axis those ramifications are located directly posterior to the great commissure. Scale bars = 25 μm.

*NP7088* covers more cells than *tdc2-GAL4* in these clusters, we compared the cell counts of the brains with double labeling by *tdc2-GAL4* and *NP7088* and those labeled with *NP7088* alone. In the VM cluster we found no significant difference between both groups (n = 9), suggesting that *NP7088* covers all VM cluster neurons labeled by *tdc2-GAL4*. In contrast, the double driver labeled two more cells in cluster AL2 than did *NP7088* alone. Thus, we conclude that *NP7088* labels a subset of the AL2 cluster cells labeled by *tdc2-GAL4*.

## Projections in the brain

The projection patterns of *tdc2-GAL4* and *NP7088* were in many parts similar to the reported OA immunoreactivity (Sinakevitch and Strausfeld, 2006). To reveal the detailed morphology of GAL4-positive neurons, we employed the *mCD8::GFP* reporter, which enables equally clear visualization of thick neurites and fine arborization (Ito et al., 2003). Despite the difference in the numbers of labeled cells (Table 1), the neuronal projections of *tdc2-GAL4* and *NP7088* are similar in many areas of the SPG (Fig. 3A,B). This may be because many of the nonoverlapping cells (e.g., cells in clusters SL and PB2) project only locally. In both lines, similar ramifications deriving from a small number of labeled neurons spread out all over the brain (Fig. 3A,B). We identified innervations in the primary gustatory center in the SOG as well as in the antennal lobes and the antennal nerves (Fig. 3C). There are also ramifications

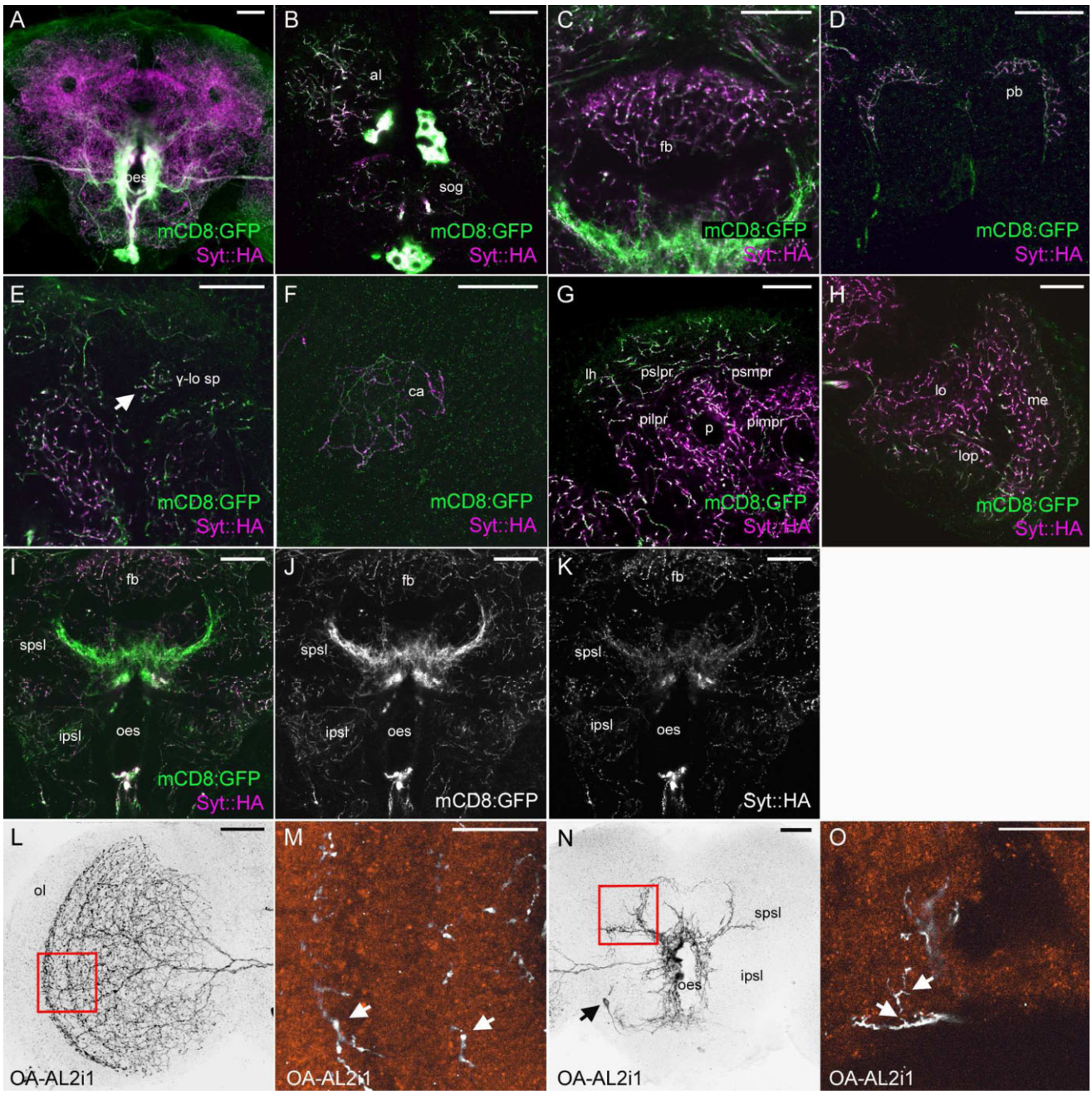


Figure 4.
**A–K:** Presynaptic regions of *tdc2-GAL4* neurons in the adult brain visualized by expressing the presynaptic marker *Syt-HA* (magenta). *UAS-mCD8::GFP* (green) labels neuronal processes of the same cells. A: Projection of confocal stacks. Syt-HA (magenta) is located throughout the central brain. Compared to other brain regions, dense processes (green) surrounding the esophagus foramen (oes) are labeled less intensively by Syt-HA. B–H: Single optical sections of distinct brain regions. The presynaptic marker Syt-HA generally labels varicose nerve terminals. B–D: The antennal lobes (al), the SOG (sog), as well as the fan-shaped body (fb) and the protocerebral bridge (pb) contain numerous neuronal terminals decorated with Syt-HA. E,F: Magnification of the mushroom body. The Syt-HA signal is detected in the spurs of the γ-lobes (γ-lo sp; arrow) and the calyces (ca), but not in the vertical lobes and other part of the medial lobes. G: Magnification of the protocerebrum, which contains abundant Syt-HA signal. lh: the lateral horn; pslpr: the posterior superior lateral protocerebrum; psmpr: the posterior superior medial protocerebrum; pilpr: the posterior inferior lateral protocerebrum; pimpr: the inferior medial protocerebrum. H: Syt-HA is entirely colocalized to nerve terminals in the lobula (lo), the lobula plate (lop), and the medulla (me) in the optic lobe. I–K: Single optical sections of the posterior slope. α-GFP and α-HA signals are presented separately in J and K, respectively Syt-HA, compared to the signal of mCD8::GFP, is less enriched in the superior (spsl) and inferior (ipsl) posterior slopes. **L–O:** Polarized morphology of cell type OA-AL2i2. Projections of confocal stacks illustrating the optic lobes and the posterior slope (L,N). The red boxes indicate the magnified areas in the corresponding close up images in M and O. Ramifications of OA-AL2i1 are monitored by mCD8::GFP (white) in the neuropil staining (orange). L,M: Varicose nerve terminals (arrows) in the optic lobe. N,O: In the posterior slope OA-AL2i1 develops spiny ramifications (arrows in O). The black arrow in N indicates a different cell labeled at the same time as OA-AL2i1. It innervates the anterior subesophageal ganglion. Scale bars = 25 μm in A–L,N; 10 μm in M,O.

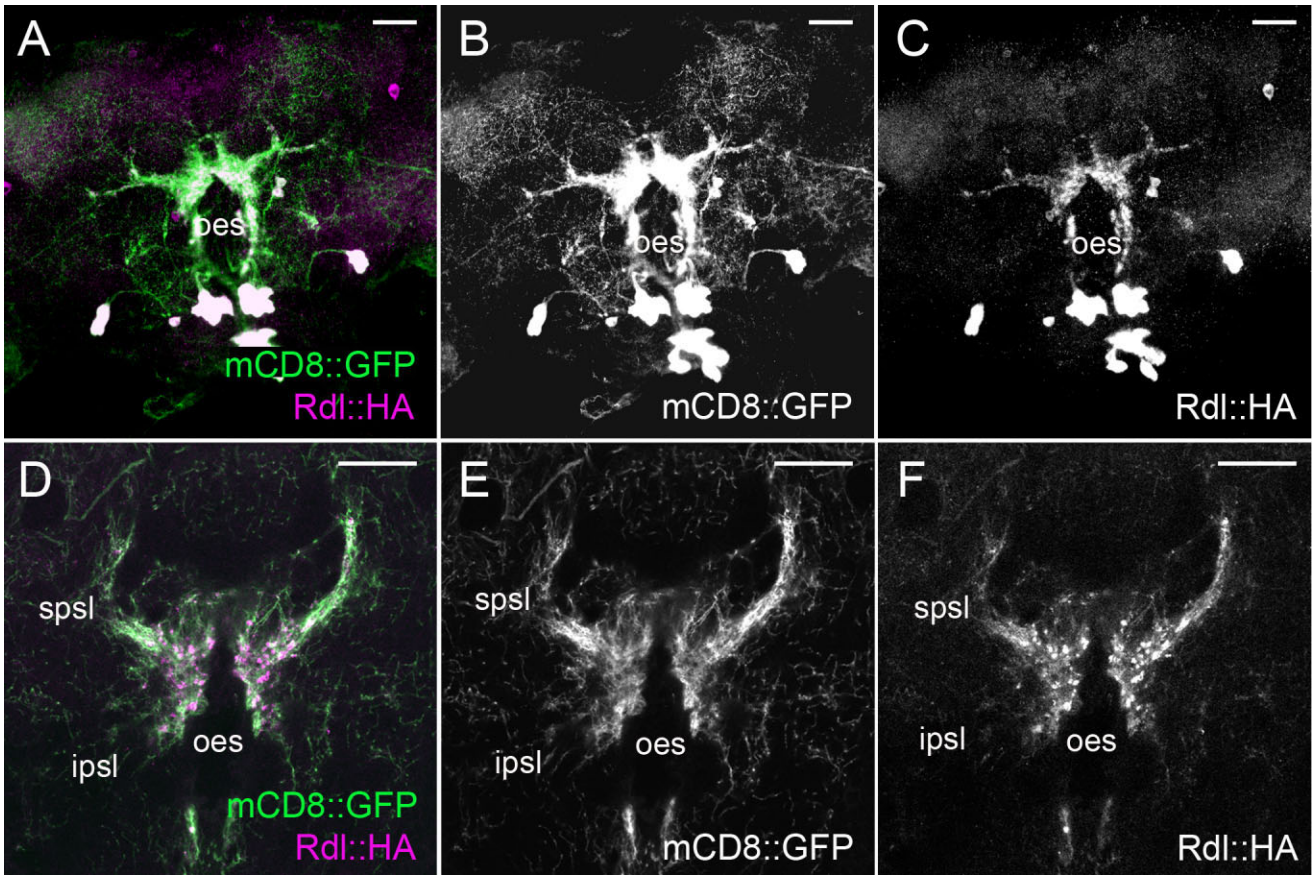


Figure 5.
Putative input regions of *tdc2-GAL4* neurons in the adult brain visualized by the postsynaptic marker *UAS-Rdl-HA* (magenta). The membrane marker *UAS-mCD8::GFP* (green) is coexpressed to visualize the entire neuronal processes. **A–C:** Projection of confocal stacks in the central brain. $\alpha$-GFP and $\alpha$-HA signal are presented separately in B and C, respectively. Rdl-HA is highly enriched in the processes surrounding the esophagus (oes) foramen. Accumulation of Rdl-HA was detected also in cell bodies. **D–F:** Single optical sections of the posterior slope. $\alpha$-GFP and $\alpha$-HA signal are presented separately in E and F, respectively. The postsynaptic marker Rdl-HA predominantly colocalizes with spiny arborizations in the posterior slope (spsl, ipsl) surrounding the esophagus (oes) foramen, implying the posterior slope as a main input area. Scale bars = 25 $\mu$m.



in the medulla, lobula, and lobula plate of the optic lobes (Fig. 3D). In the mushroom body, innervations are restricted to the calyx (Fig. 3E), the $\gamma$-lobe (Fig. 3F) and the spur of the $\gamma$-lobe (Fig. 3G; see also Tanaka et al., 2008). There was no detectable signal in other parts of the mushroom body, such as the pedunculus and the $\alpha/\beta$ lobes (Fig. 3G,H). In the central complex, labeled processes are present in the fan-shaped body (Fig. 3I), the protocerebral bridge (Fig. 3J), and weakly in the nodulli (Fig. 3I), but absent in the ellipsoid body (Fig. 3K). Furthermore, there is innervation all over the superior, inferior, and lateral protocerebra including the lateral horn and ventrolateral protocerebrum (Fig. 3H). Conspicuously dense ramifications surround the esophagus in the posterior slope (Fig. 3L).

## Localized postsynaptic regions of octopaminergic neurons

The terminal structures of these neurons show that they are highly polarized: Spiny arbors are enriched in the posterior slope, and bouton-like terminals are distributed in spatially distinct areas of the brain (see Fig. 4L–O, and single-cell morphology, below). The polarized morphology implicates their functions as post- and presynapses, respectively. To corroborate this morphological polarity with genetic markers, we expressed proteins predominantly accumulating in pre- and postsynaptic sites: HA-tagged Synaptotagmin (Syt-HA; Fig. 4) and the HA-tagged subunit of the ionotropic GABA-receptor Resistance-to-Dieldrin (Rdl-HA; Fig. 5), respectively (Robinson et al., 2002; Sanchez-Soriano et al., 2005). As expected, Syt-HA predominantly, but not exclusively, labels the varicose terminals of GAL4-positive neurons throughout the brain (Fig. 4). Although the specificity of the localization of Rdl-HA for GABAergic postsynapses is still unclear, it predominantly labeled the dense arbors of GAL4-expressing neurons that surround the esophagus in the posterior slope, posterior to the great commissure (Fig. 5). This region corresponds to the spiny terminals (Fig. 4N,O), where the presynaptic marker Syt-HA is poorly localized (Fig. 4I,K). These results suggest that the majority of GAL4-positive neurons receive synaptic inputs in the posterior slope surrounding the esophagus foramen. The output regions seem to be

TABLE 3. Number of Samples Examined for Each Cell Type in *tdc2-GAL4* and *NP7088*

| Cell type | *tdc2-GAL4* (n=1060) | *NP7088* (n=747) |
|---|---|---|
| OA-AL2i1 | 27 | 2 |
| OA-AL2i2 | 66 | 8 |
| OA-AL2i3 | 37 | 4 |
| OA-AL2i4 | 12 | 2 |
| OA-AL2b1 | 2 | 2 |
| OA-AL2b2 | — | 51 |
| OA-VPM1 | 131 | 12 |
| OA-VPM2 | 7 | — |
| OA-VPM3 | 34 | 6 |
| OA-VPM4 | 5 | 10 |
| OA-VPM5 | 2 | — |
| OA-VUMa1 | 138 | 23 |
| OA-VUMa2 | 100 | 28 |
| OA-VUMa3 | 99 | 7 |
| OA-VUMa4 | 35 | 16 |
| OA-VUMa5 | 4 | — |
| OA-VUMa6 | 5 | 3 |
| OA-VUMa7 | 2 | 1 |
| OA-VUMa8 | 2 | 9 |
| OA-VUMd1 | 13 | 1 |
| OA-VUMd2 | 12 | 5 |
| OA-VUMd3 | 12 | 5 |
| OA-VL1 | 26 | — |
| OA-VL2 | 21 | — |
| OA-ASM1 | 20 | — |
| OA-ASM2 | 19 | — |
| OA-ASM3 | 100 | — |

distributed widely in the brain and segregated from the major input region.

## Morphology of single octopaminergic neurons

The ramification of the labeled neurons is so complex that terminals are not traceable to individual neurons in the full set of GAL4-expressing cells. To determine the projection patterns of individual octopaminergic neurons we carried out a large-scale morphological analysis of Flp-out clones (Wong et al., 2002) using *tdc2-GAL4* and *NP7088* (see Materials and Methods). We analyzed 1060 specimens in *tdc2-GAL4* and 747 in *NP7088* (Table 3). In total, we identified 27 types of octopaminergic neurons in the SPG and SOG. The majority of cell types were repeatedly labeled in both GAL4 lines, although the labeling frequency of certain neurons in clusters AL2 and VM was low (Table 3).

The neurites and terminal areas of each type revealed an unexpected stereotypy across individual preparations (see Fig. 14). We also found that the clear morphological polarity of spiny arbors and varicose terminals is characteristic of the majority of single neurons we analyzed (e.g., Fig. 4L–O). In the following we present a representative example of each type of GAL4-expressing octopaminergic neurons. We exclusively describe neurons belonging to OA-immunoreactive cell clusters, i.e., AL2, VM, VL, and ASM. For each cluster we evaluate whether we identified the complete set of cell types by comparing the labeling frequency with the total cell number.

Because we named each single OA-immunoreactive neuron according to their locations, we add a prefix "OA-" to distinguish them from other neurons that are located in similar areas. Such single identified cells may in the future be given similar names based, again, on their positions.

## Antennal lobe cluster neurons (OA-AL2)

Among eight cells in cluster AL2 in *tdc2-GAL4*, we identified at least six different cell types. Four of them send projections to the ipsilateral optic lobe; we named them OA-AL2i1-4 (Fig. 6). The other two types bilaterally project to both optic lobes, which we named OA-AL2b1 and b2 (Fig. 7). Among them OA-AL2b2 was not confirmed to be octopaminergic (see below).

The labeling frequency of cells in cluster AL2 varied depending on the cell types (Table 3). For example, OA-AL2i2 and OA-AL2i3 were labeled frequently, which might imply that these cell types comprise more than one cell. In contrast, OA-AL2b1 was found only twice in 1,060 samples (Table 3), implying that some cell types in this cluster have not been visualized in our analysis.

The projection of individual AL2 cluster neurons was stereotypic. For example, OA-AL2i1 in different samples exhibits a consistent projection pattern (Fig. 14A–L). Since the stereotypy was observed in all the investigated octopaminergic neurons, the identification of cell types was straightforward.

The somata of cluster AL2 are located ventromedial to the antennal lobe (Fig. 3C). All neurons in this cluster exhibit a highly polarized structure. They send one neurite along the esophagus foramen to the posterior slope, where they branch out. They typically form spiny arborizations in the posterior slope surrounding the esophagus foramen (Figs. 4N,O, 6B,F,J,N). In the case of OA-AL2i1, OA-AL2i2, and OA-AL2i3, such ramifications extend ipsilaterally into the posterior lateral and ventromedial protocerebra (Fig. 6B,G,K). OA-AL2i1 additionally innervates the posterior inferior medial protocerebrum. In the posterior slope, ventrolateral to the esophagus foramen, secondary processes of all OA-AL2i neurons emerge to target the ipsilateral optic lobe (Fig. 6B,F,J,N). From this neurite, fine processes branch off and form varicosities in the ventral inferior posterior slope (Fig. 6O).

In the optic lobes, OA-AL2i1-4 form varicose nerve terminals in specific regions (Figs. 4L,M, 6D,H,L,P). OA-AL2i1 innervates the entire optic lobe except for the lamina (Fig. 6D). OA-AL2i2 ramifies in the lobula and the inner medulla (Fig. 6H). OA-AL2i3 and OA-AL2i4 exhibit nerve endings in the outer (Fig. 6L), and inner medulla (Fig. 6P), respectively. In one cell type (OA-AL2i1) branches innervate the protocerebral bridge (Fig. 6C).

OA-AL2b1 and OA-AL2b2 (Fig. 7) possess an additional character: secondary neurites bilaterally innervate both optic lobes (Fig. 7A,D). The bifurcated processes of OA-AL2b1 arise from ramifications of the dorsolateral esophagus foramen and target the lobulae (Fig. 7B,C). Additionally, collateral branches emerge from these neurites and form varicose terminals in the posterior lateral, posterior inferior lateral, and ventrolateral protocerebra (Fig. 7B). Processes of OA-AL2b2 emerge at the ventrolateral esophagus foramen (Fig. 7E), and ramify in the outer medullae (Fig. 7F). Because not all neurons in cluster AL2 of *NP7088* are OA-immunoreactive, and because OA-AL2b2 was identified in *NP7088*, but not in *tdc2-GAL4*, this cell type might not be octopaminergic.

## Cellular composition of the VM cluster

The VM cluster neurons can be categorized into two groups according to the pathway of their primary neurites: ventral paired median neurons (OA-VPM) and ventral unpaired median neurons (OA-VUM; Fig. 1H).

Somata of OA-VPM neurons are localized slightly lateral to the midline (Fig. 1H). Their primary neurites run apart from the

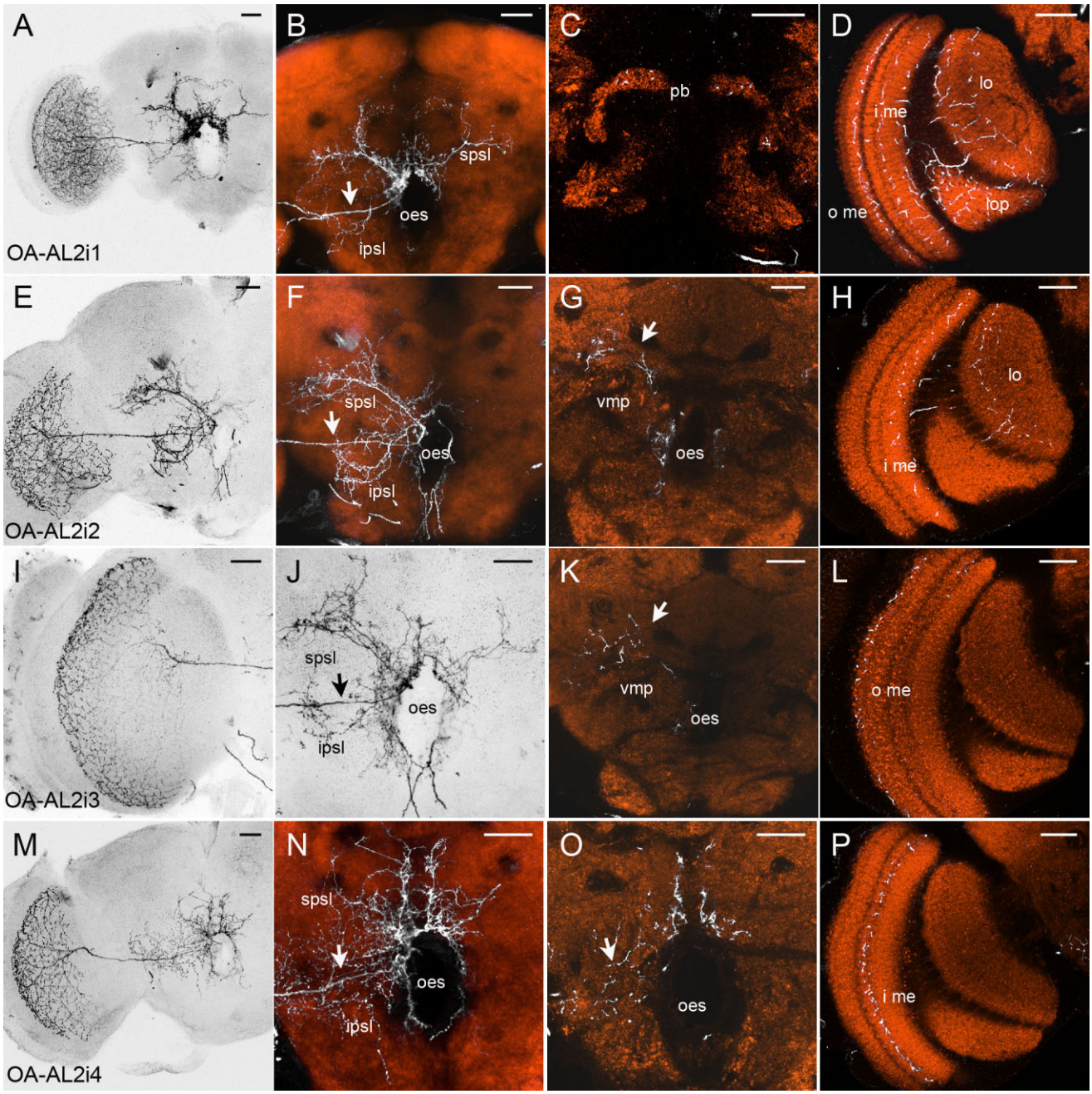


Figure 6.
Single-cell staining of OA-AL2i neurons. Each row indicates a specific cell type generated by Flp-out clones. The left-most column depicts projections of confocal stacks illustrating the overall projection patterns of the respective cell types in a frontal view. Right columns depict characteristic ramifications of each cell type monitored by mCD8::GFP (white) in the neuropil staining (orange). All OA-AL2i neurons form spiny arborizations in the posterior slope (spsl; ipsl) surrounding the esophagus foramen (oes; see A,B,E,F,J,M,N) with thick single axon projecting laterally to the optic lobe (arrows in B,F,J,N). **C:** In the central brain OA-AL2i1 exhibits additional innervation in the protocerebral bridge (pb). **D:** In the ipsilateral optic lobe OA-AL2i1 ramifies in the lobula (lo), lobula plate (lop), the inner (i me) and outer medulla (o me). **G:** OA-AL2i2 extends arbors into the ipsilateral ventromedial protocerebrum (vmp; arrow). **H:** In the ipsilateral optic lobe OA-AL2i2 innervates the inner medulla (i me) and the lobula (lo). **K:** Arborizations of OA-AL2i3 extend into the ipsilateral ventromedial protocerebrum (arrow). **L:** OA-AL2i3 ramifies in the ipsilateral outer medulla (o me). **O:** Similar to all other OA-AL2i-neurons, OA-AL2i4 forms varicose terminals in the ipsilateral inferior posterior slope (ipsl, arrow). **P:** OA-AL2i4 targets the ipsilateral inner medulla (i me). Scale bars = 25 $\mu$m.

median tracts toward the ventral esophagus (Fig. 1H). They develop asymmetric ramifications in the brain and SOG (Fig. 8).

OA-VUM neurons send their primary neurites via one of three median tracts along the anteroposterior axis (Fig. 1G,H). These neurites follow the tracts toward the posterior ventral

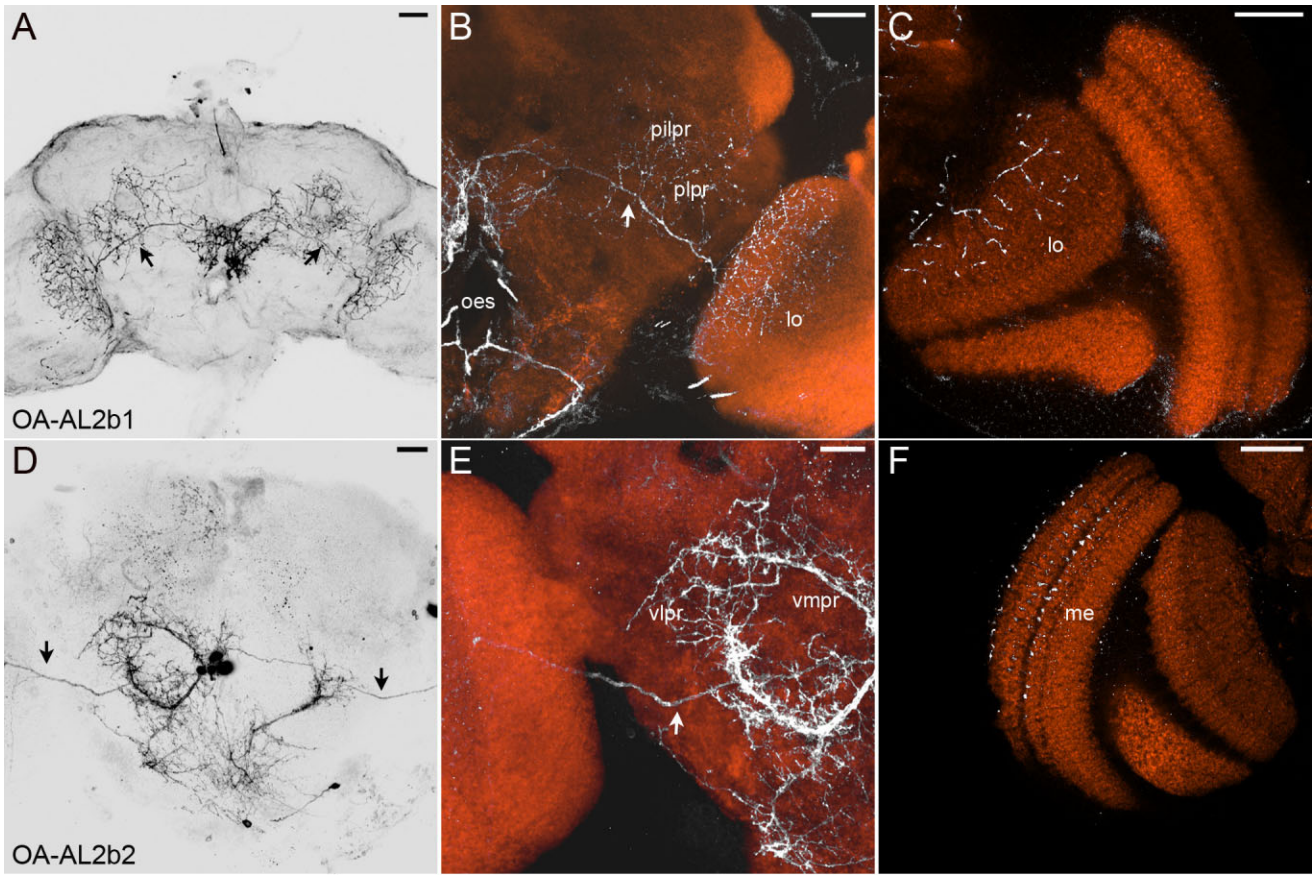


Figure 7.
Single-cell staining of OA-AL2b neurons. The panels and the color scheme are organized as in Figure 6. OA-AL2b1 and OA-AL2b2 bilaterally innervate the optic lobes (arrows). **B:** The processes of OA-AL2b1 to the optic lobes (arrow) have collaterals in the posterior lateral protocerebrum (plpr) and posterior inferior lateral protocerebrum (pilpr). **C:** Innervation of OA-AL2b1 in the lobula (lo). **E:** OA-AL2b2 has spiny arborizations in the ventrolateral (vlpr) and the ventromedial protocerebrum (vmpr). **F:** OA-AL2b2 innervates the outer layer of the medulla (me). Scale bars = 25 $\mu$m.

area of the esophagus foramen where they symmetrically branch out to innervate the CNS (i.e., the SPG, SOG, and thoracicoabdominal ganglia) (Figs. 1G, 8–11). Despite some exceptions, the midline neurite is the hallmark of octopaminergic VUM neurons across different insect species (Bräunig and Pflüger, 2001).

Figure 8.
Single-cell staining of OA-VPM neurons. The panels and the color scheme are organized as in Figure 6. To the right we depicted characteristic ramifications of each cell type in the central brain. **A–D:** Innervations of OA-VPM1 in the central brain (A–C) and the thoracicoabdominal ganglion (D). B: OA-VPM1 develops varicose ramifications in the SOG (sog). C: Varicose terminals of OA-VPM1 extend in the ventromedial protocerebrum (vmpr). From the ventrolateral esophagus a thick axon runs laterally into the ipsilateral half (arrow), projecting into the cervical connectives. D: Innervations of OA-VPM1 in the ventral nerve cord. Terminals are present in the thoracic ganglia 1–3 (tg1-3) and the abdominal ganglia (ag). **E–H:** Innervations of OA-VPM2. F: Ramifications in the contralateral antennal nerve (an) and SOG (sog). G: Innervations in the ventrolateral protocerebrum (vlpr), the ventromedial protocerebrum (vmpr), and the anterior inferior medial protocerebrum (aimpr) in the contralateral brain hemisphere. Its primary neurite bifurcates at the ventral to the ventrolateral protocerebrum (arrow). F,H: Ipsilateral ramifications in the SOG (sog) and the posterior slope (spsl). **I–L:** Innervations of OA-VPM3. J: A conspicuous neurite of OA-VPM3 (arrow) projects from the anterior ventrolateral esophagus (oes) to the anterior superior medial protocerebrum (asmpr) passing the posterior margin of the antennal lobe (al). At the posterior brain it crosses the midline in the middle superior medial protocerebrum (smpr; arrowhead). OA-VPM3 exhibits varicose ramifications in the superior protocerebrum, and the fan-shaped body (fb). K: Innervation in the contralateral $\gamma$-lobe spur ($\gamma$-lo sp). L: Ramifications in the contralateral calyx (ca). **M–P:** Innervations of OA-VPM4. N: A thick neurite (arrow) projects along the posterior margin of the antennal lobe (al) to the anterior superior medial protocerebrum (asmpr). It forms varicose ramifications in the contralateral superior (asmpr, aslpr), inferior (aimpr, ailpr), and ventrolateral protocerebra (vlpr). O: It crosses the midline dorsal to the fan-shaped body (fb, arrow) and targets the ipsilateral inferior lateral protocerebrum (milpr) where it forms varicose arborizations. P: Dense innervations in the contralateral spur of the $\gamma$-lobe ($\gamma$-lo sp). **Q–T:** Innervations of OA-VPM5. R: Innervation in the antennal lobe (al) in one brain hemisphere provides a small process crossing the midline. It ramifies sparsely in opposing antennal lobe (arrow). S,T: OA-VPM5 projects through the inner antennocerebral tract (arrow) to the lateral horn (lh) and the calyx (ca) of the mushroom body. Scale bars = 25 $\mu$m.

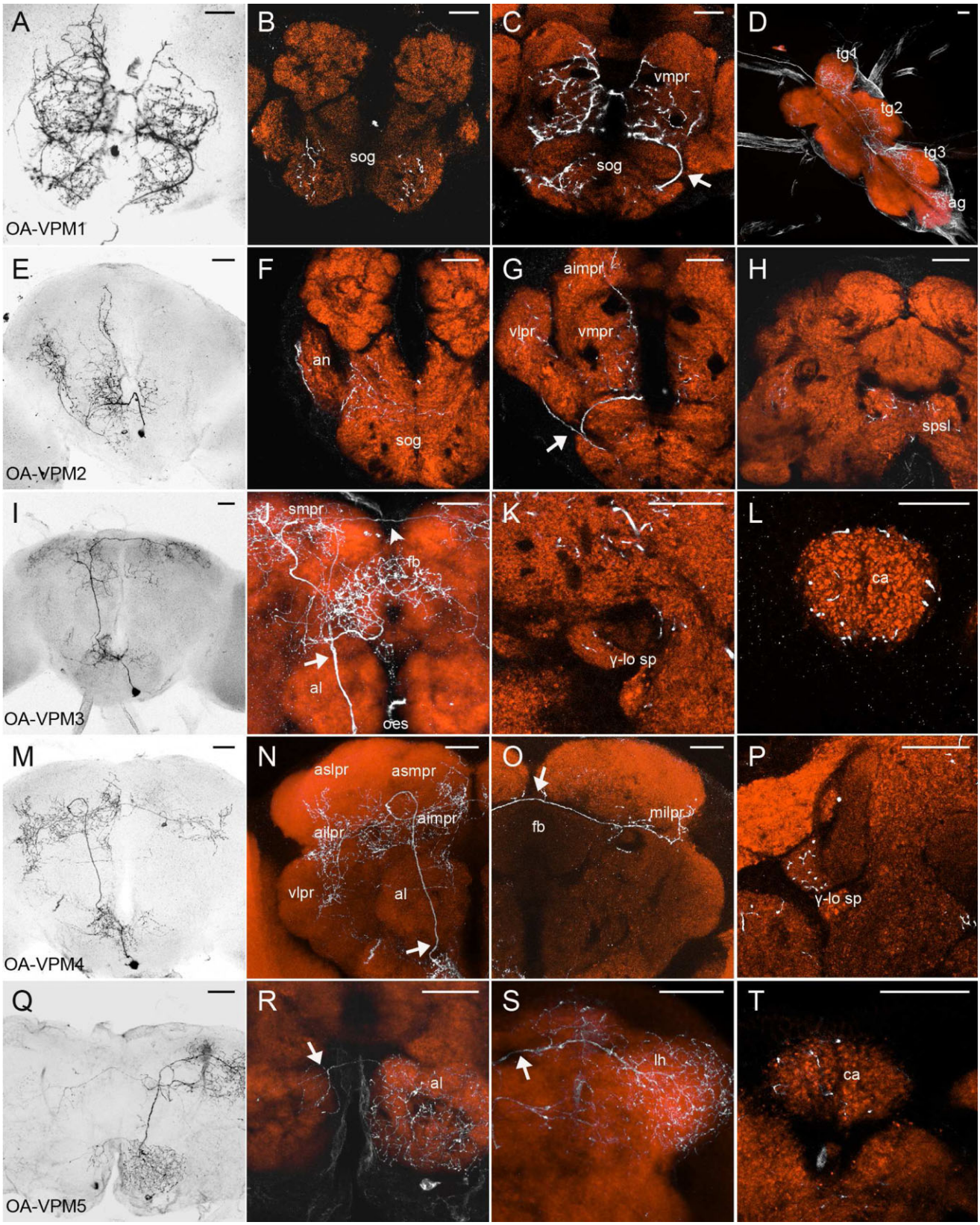


Figure 8

We further classified the VUM neurons into two classes: OA-VUMa and OA-VUMd. OA-VUMa neurons have ascending processes projecting from the SOG to the SPG. OA-VUMd neurons, in addition to their ascending profiles, have descending processes projecting through the cervical connective to the thoracicoabdominal ganglia.

We identified five types of VPM neurons, eight types of VUMa neurons, and three types of VUMd neurons. Like cells in the AL2 cluster, the projection of VM cluster neurons was stereotypic. Given that each type of the VPM neurons consists of a pair of cells, we identified at least 21 of the 27 OA-immunoreactive neurons located along the ventral midline of *tdc2-GAL4*. Concerning the remaining six cells, it is possible that some cell types may consist of multiple cells, because some neuron types were much more frequently labeled than the others (e.g., OA-VUMa1 labeled 138 times; Table 3). Also, as discussed in the previous section, we might have failed to visualize certain cell types, given that some VM cluster neurons (e.g., OA-VPM5, OA-VUMa7, and OA-VUMa8) are labeled only twice in 1,060 samples (Table 3). Further investigation is required to distinguish these two possibilities.

In the following, we describe the morphology of single VM cluster neurons, beginning with the OA-VPM neurons, then moving to the OA-VUM neurons.

## Ventral paired median neurons (OA-VPM)

OA-VPM neurons (Fig. 8) belong to the VM cluster, but do not exhibit a mirror symmetric innervation pattern like OA-VUM neurons. They are paired neurons that develop complementary projections in the SPG and the SOG. All identified OA-VPM neurons exhibit a polarized structure; spiny arborizations in the posterior slope surrounding the esophagus foramen and varicose terminals in distinct target regions in the brain. The primary neurites of all OA-VPM neurons (except for OA-VPM5) project dorsally and remain separate from the median tracts of the OA-VUM neurons (Fig. 1H).

The cell body of OA-VPM1 (Fig. 8A–D) is located at the anterior margin of the SOG, anterior and lateral to the subcluster VMmd. Its primary neurite projects along the ventral esophagus and ramifies bilaterally in the ventromedial protocerebrum (Fig. 8C). Whereas the position of the cell body, the projection patterns of the primary neurite, and the descending secondary neurite are clearly asymmetric, its main arborizations in the SPG and SOG are mirror-symmetric. OA-VPM1 forms varicose nerve terminals in the SOG and the ventromedial protocerebra (Fig. 8B,C). The descending secondary neurite of OA-VPM1 (Fig. 8C,D) emerges from the ventrolateral esophagus laterally into the ipsilateral half of the SPG, and turns ventrally to descend through the cervical connective (Fig. 8C, arrow). The descending axon terminates in all three ipsilateral thoracic neuromeres and the abdominal neuromere (Fig. 8D). As a representative example of stereotypy, the projection of OA-VPM1 in three different samples is shown in Figure 14M–U.

OA-VPM2 (Fig. 8E–H) has its cell body localized slightly lateral to the ventral midline and possibly belongs to the VMmd subcluster. The primary neurite runs to the area around the ventral esophagus foramen where it crosses the midline (Fig. 8E). It then bifurcates at the ventral part of the contralateral ventrolateral protocerebrum (Fig. 8G). The emerging branches are the source of contralateral ramifications in the antennal nerve, ventrolateral, ventromedial, anterior inferior medial protocerebra, and the SOG (Fig. 8E–G). To a small extent, OA-VPM2 innervates the ipsilateral SOG as well (Fig. 8F).

The soma of OA-VPM3 (Fig. 8I–L) is located lateral to the subcluster VMmx. Its primary neurite projects to the ventral esophagus, where it crosses the midline. Then it passes the posterior margin of the contralateral antennal lobe and runs further dorsally to the anterior superior medial protocerebrum. There it turns posteriorly and medially to cross the midline again and to terminate in the ipsilateral middle superior medial and lateral protocerebra (Fig. 8J). OA-VPM3 exhibits branches successively protruding from the major neurite (Fig. 8J). They terminate in parts of the contralateral superior medial and lateral protocerebra, the fan-shaped body, the contralateral noduli, and the contralateral mushroom body, i.e., in the spur and the outer region of the calyx (Fig. 8J–L).

OA-VPM4 (Fig. 8M–P) is located posterior and slightly lateral to the subcluster VMlb. It sends an axon to the anterior ventral esophagus where it crosses the midline. Its secondary neurite shares the tract with that of OA-VPM3, running further along the posterior margin of the antennal lobe to the anterior superior medial protocerebrum (Fig. 8M,N, arrow). There it turns posteriorly and medially, crossing the midline again along the dorsal margin of the fan-shaped body (Fig. 8O, arrow). OA-VPM4 ramifies in the contralateral brain hemisphere, i.e., in the superior, inferior, and ventrolateral protocerebra, and the $\gamma$ lobe and the spur of the mushroom body (Fig. 8N–P). In addition, it projects to the SOG (Fig. 8M,N). In the ipsilateral brain hemisphere, the axon of OA-VPM4 terminates in the middle inferior lateral and middle inferior medial protocerebrum (Fig. 8O).

As of OA-VPM4, the cell body of OA-VPM5 (Fig. 8Q–T) is located slightly lateral to the cluster VMlb. However, because of unclear neuropil staining in this sample the separate projection of its primary neurite from the median tract could not be determined. We categorized OA-VPM5 to the paired midline neurons because of its asymmetric innervation (Fig. 8Q). It innervates the antennal lobe (Fig. 8R) and sends a single neurite through the inner antennocerebral tract (iACT) to the lateral horn (Fig. 8S, arrow). Collaterals innervate the calyx of the mushroom body (Fig. 8T). The projection pattern of OA-VUMa2 and OA-VPM5 are similar (Figs. 8Q–T, 9E–H), although OA-VPM5 exhibits an asymmetric innervation pattern. OA-VPM5 also ramifies sparsely in the contralateral antennal lobe (Fig. 8R). The contralateral ramification arises from a small process which crosses the midline dorsal of the antennal lobes (Fig. 8R, arrow).

## Ascending VUM neurons (OA-VUMa)

As described before, the VM cluster is segregated into three subclusters. Among them, all identified OA-VUMa neurons belong to subclusters VMmd and VMmx. These neurons have their primary neurites projecting dorsally through the median tracts (Fig. 9). They bifurcate in the area ventral to the esophagus foramen and form spiny arborizations localized in the posterior slope surrounding the esophagus (e.g., Fig. 9H,K,N,O). OA-VUMa neurons have pairs of secondary neurites that emerge from these arbors and form varicose nerve terminals in distinct brain regions.

Symmetric and complex ramifications of OA-VUMa1 (Fig. 9A–D) extend throughout the ventromedial protocerebra (Fig. 9B,C), i.e., to the posterior margins of the antennal lobes and

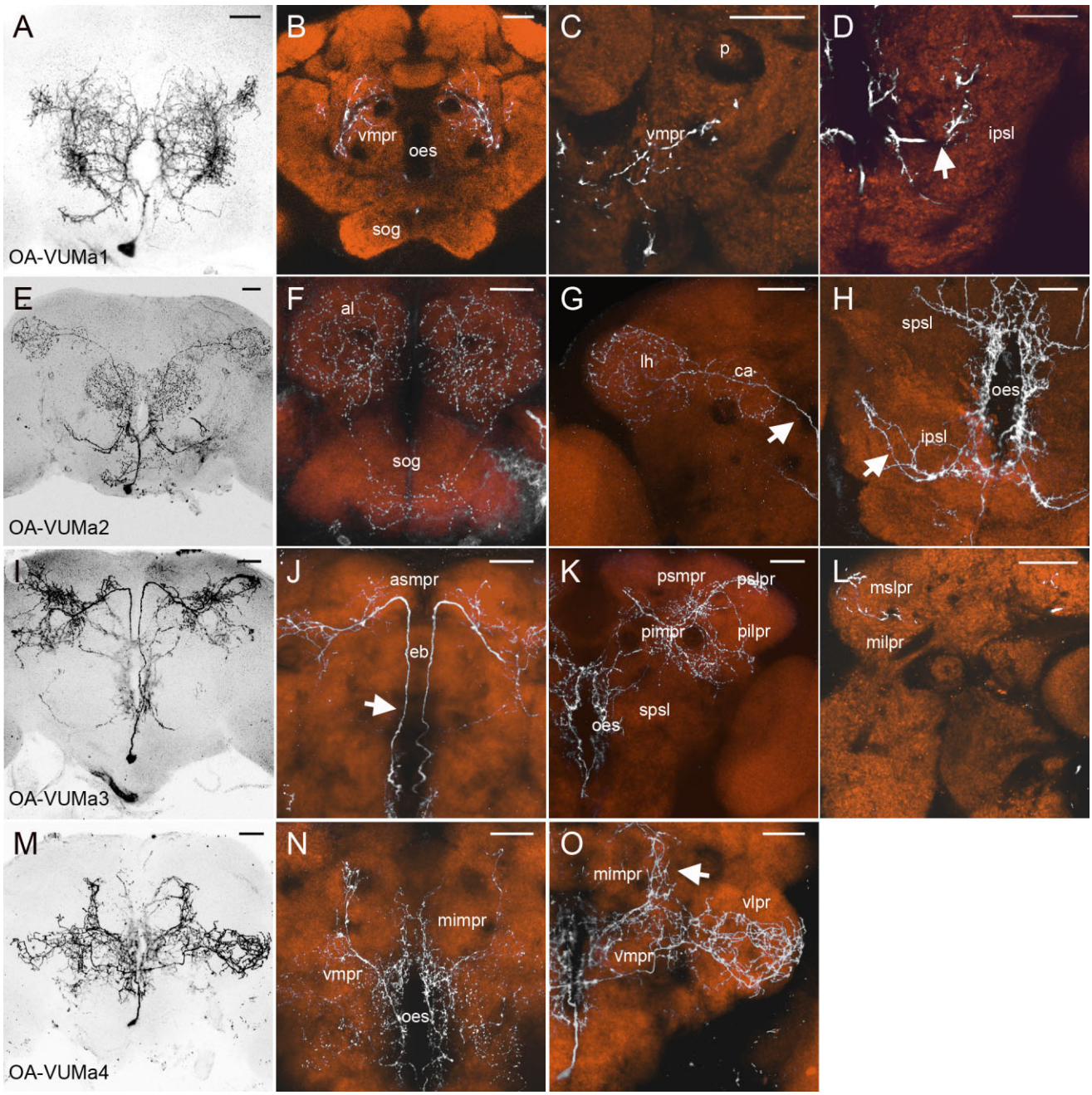


Figure 9.
Single cell morphology of ascending OA-VUM neurons. The panels and the color scheme are organized as in Figure 6. **A,B:** Varicose arborizations of OA-VUMa1 in the ventromedial protocerebrum (vmpr) just posterior to the antennal lobes. **C:** Ramifications of OA-VUMa1 extend to the ventral margin of the pedunculus (p). **D:** A distinct branch of OA-VUMa1 ramifies in the inferior posterior slope (ipsl, arrow). **E,F:** Innervation of OA-VUMa2 in the antennal lobes (al) and the subesophageal ganglion (sog) with varicose terminals. **E,G:** OA-VUMa2 projects through the inner antennocerebral tract (arrow) and terminates in the lateral horn (lh) and the calyx (ca) of the mushroom bodies with varicose endings. **H:** Spiny arborizations of OA-VUMa2 are located around the esophagus foramen and extend into the posterior slope (ispsl, spsl; arrow). **I,J:** OA-VUMa3 sends a parallel pair of large secondary neurites (arrow) from the ventral esophagus to the anterior superior medial protocerebrum (asmpr). They bypass the anterior margin of the ellipsoid body (eb). **K:** Varicose ramifications of OA-VUMa3 extend into the posterior protocerebrum (psmpr, pslpr, pimpr, pilpr). Spiny arborizations are localized around the esophagus foramen. **I,L:** One branch of OA-VUMa3 innervates the middle lateral protocerebrum (milpr, mslpr). **M–O:** OA-VUMa4 ramifies in the ventrolateral protocerebrum (vlpr) and the ventromedial protocerebrum (vmpr) where it forms varicose nerve terminals. One characteristic branch enters the middle inferior medial protocerebrum (mimpr, arrow). Spiny arborizations of OA-VUMa4 extend around the esophagus (oes) foramen in the posterior slope. Scale bars = 25 $\mu$m.

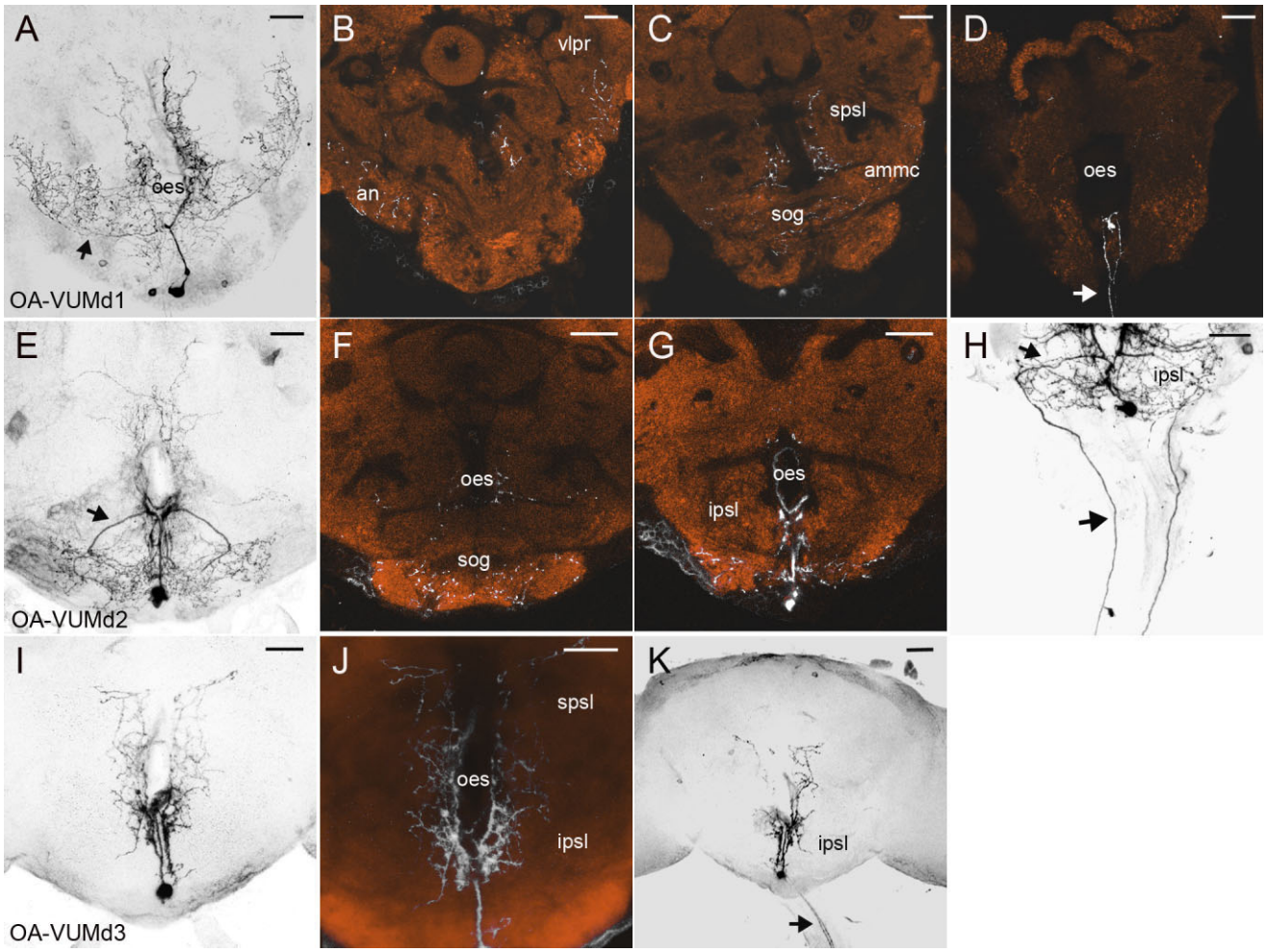


Figure 10.
Single-cell staining of descending OA-VUM neurons. The panels and the color scheme are organized as in Figure 6. **A,B:** Bifurcated neurites of OA-VUMd1 (arrow) from the ventral esophagus (oes) ramify in the ventrolateral protocerebrum (vlpr) and the antennal nerve (an). **C:** OA-VUMd1 innervates the SOG (sog) and the antennal motor and mechanosensory center (ammc). **D:** A pair of descending axons of OA-VUMd1 project from the ventral esophagus into the cervical connectives (arrow). **E–H:** The secondary neurites of OA-VUMd2 (arrow) project from the ventral esophagus (oes) to the lateral inferior posterior slope (ipsl, H). H: The secondary neurites descend out to the connectives (arrows). F,G: Varicose terminals of OA-VUMd2 are located in the SOG (sog) and the inferior posterior slope (ipsl). **I–K:** OA-VUMd3 forms spiny arborizations in the posterior slope (J, spsl and ipsl) surrounding the esophagus (oes) foramen. K: A pair of descending neurites emerge from the midline of the esophagus foramen (arrow). Scale bars = 25 $\mu$m.

the ventral margins of the mushroom body pedunculi (Fig. 9C). A distinct branch, originating from the neuropil area ventrolateral to the esophagus foramen, supplies the inferior posterior slope with varicose nerve terminals (Fig. 9D).

OA-VUMa2 (Fig. 9E–H) sends symmetric secondary neurites from the area around the ventrolateral esophagus foramen to the posterior margins of the antennal lobes, where both neurites bifurcate. One branch ramifies within the antennal lobe and runs further to the anterior SOG (Fig. 9F). The second branch enters the iACT, the trajectory of the olfactory projection neurons that connect the antennal lobes with the calyx and the lateral horn (Fig. 9G, arrow). In addition, OA-VUMa2 has numerous terminals in the lateral horn with collaterals to the calyx of the mushroom body (Fig. 9G).

Symmetric secondary neurites of OA-VUMa3 (Fig. 9I–L) project dorsally, bypassing the anterior margin of the ellipsoid body (Fig. 9J, arrow). In the anterior superior medial protocerebrum, these neurites turn laterally and posteriorly (Fig. 9J). They ramify densely in the superior posterior slope and the posterior protocerebrum surrounding the mushroom body pedunculi (Fig. 9K). One branch innervates the middle lateral protocerebrum as well (Fig. 9L).

OA-VUMa4 (Fig. 9M–O) extensively ramifies in the ventrolateral and ventromedial protocerebra. One characteristic branch enters and ramifies in the middle inferior medial protocerebrum, right between the fan-shaped body and the pedunculus (Fig. 9N,O, arrow).

## Descending VUM neurons (OA-VUMd)

We identified three types of OA-VUM neurons with both descending and ascending processes (Fig. 10). Judging from their primary neurites, all descending OA-VUM neurons ap-

pear to belong to cluster VMlb. At the area around the ventral esophagus foramen, they branch and typically form a pair of secondary neurites that descend through the cervical connective (Fig. 10D,H,K, arrows). Arguably, they target the thoracicoabdominal ganglia. In addition, all descending OA-VUM neurons show a similar morphological polarity as ascending OA-VUM neurons: all of them form spiny arborizations in the posterior slope surrounding the esophagus and varicose nerve terminals in their target regions.

OA-VUMd1, in a frontal view, exhibits a fan-shaped projection pattern in the brain (Fig. 10A). Two laterally projecting neurites (Fig. 10A, arrow) ramify in the ventrolateral protocerebrum (Fig. 10B), the antennal nerve (Fig. 10B), and the SOG (Fig. 10C). In addition, this neuron innervates a specific area in the SPG, supposedly the antennal mechanosensory and motor center (Fig. 10C).

The secondary neurites of OA-VUMd2 (Fig. 10E–H) project from the area around the ventral esophagus foramen to the lateral inferior posterior slope where they turn ventrally and enter the cervical connective (Fig. 10H, arrows). OA-VUMd2 develops varicose nerve terminals in the posterior SOG (Fig. 10F) and the inferior posterior slope (Fig. 10G). Similar to the case of OA-VUMa3, we found no sample where OA-VUMd2 was labeled alone. Therefore, its innervation pattern in the brain remains ambiguous.

The secondary neurites of OA-VUMd3 emerge from the area around the ventral esophagus foramen and project directly through the cervical connectives. As in the case of the other OA-VUM neurons, OA-VUMd3 forms spiny ramifications in the posterior slope, but does not seem to innervate other parts of the SPG or the SOG (Fig. 10I,J). We assume that it develops varicose terminals in the thoracicoabdominal ganglia.

## Other VM cluster neurons

Our large-scale screening identified four more cell types in the VM cluster (OA-VUMa5-8). Each of them exhibits characteristic neurites whose projection patterns are distinct from those described hitherto (Fig. 11). However, these neurons were significantly underrepresented compared to other GAL4-expressing neurons (Table 3). Therefore, the detailed morphology and stereotypy of the four additional neurons remain ambiguous.

As the other VM cluster neurons, the axons emerge from ramifications surrounding the esophagus foramen in the posterior slope. Innervations of these four neurons typically cover many brain regions (except for OA-VUMa5; see below) with distinct patterns (Fig. 11).

Symmetric secondary neurites of OA-VUMa5 (Fig. 11A–C) project from the ventrolateral esophagus to the antennal lobes, where they ramify extensively (Fig. 11B). They reach the antennal lobes via the same paths as those of OA-VUMa2. Since other VM cluster neurons were always colabeled with OA-VUMa5, the description of the OA-VUMa5 terminals remains ambiguous.

OA-VUMa6 sends a pair of two major branches in each hemisphere laterally from the dorsal esophagus foramen (Fig. 11E, arrows). They ramify in the inferior and superior protocerebra.

OA-VUMa7 sends one secondary neurite along the midline from the esophagus. It bifurcates ventral to the ellipsoid body and starts to ramify in both hemispheres (Fig. 11I, arrow). This single-sided secondary neurite that projects in parallel to the midline is a unique feature of this neuron, although OA-VUMa7 shares all the common features of OA-VUM neurons (Fig. 11G,H). The emerging symmetric projections ramify in the anterior area of the medial and lateral protocerebra (Fig. 11I). In the posterior slope one neurite projects from the ventrolateral esophagus to the inferior lateral protocerebrum (Fig. 11H, arrow).

Esophagus OA-VUMa8 exhibits a pair of mirror-symmetric neurites projecting from the area around the ventral esophagus to the anterior. It further branches in the ventromedial protocerebrum, more specifically ventrolateral to the iACT (Fig. 11K,L, arrows). Profuse arbors cover the ventrolateral and superior medial protocerebra, respectively.

## Neurons of the ventrolateral protocerebrum cluster (OA-VL)

In each brain hemisphere of *tdc2-GAL4*, there are two OA-immunoreactive somata between the antennal lobe and the ventrolateral protocerebrum. Single-cell staining revealed two different cell types in this cluster (OA-VL1 and OA-VL2; Fig. 12). Both types send a process to the SOG where it crosses the midline (Fig. 12B,E,F). Bilateral ramifications of these neurons reach the antennal nerves and the SOG (Fig. 12B,E,F). On the ipsilateral side ramifications extend to the inferior lateral and ventrolateral protocerebra.

Each cell type has a descending axon that diverges from the main neurite medial to the antennal nerve (Fig. 12B,E, arrows) but they differ in their projection patterns. In the case of OA-VL1, the descending fiber projects through the SOG and the connective (Fig. 12B) to innervate the ipsilateral side of all three thoracic neuromeres (Fig. 12C). The branch of OA-VL2 runs posteriorly along the lateral margin of the SOG (Fig. 12E, arrow). We were unable to trace its trajectory to the thoracicoabdominal ganglia. OA-VL1 and OA-VL2 differ only in the trajectory of a single neurite. We repeatedly found one or the other cell type (i.e., 26 and 21 samples for OA-VL1 and OA-VL2, respectively; Table 3), suggesting that they are different cell types.

## Neurons of the anterior superior medial protocerebrum (ASM)

In both hemispheres, there are ≈8 OA-immunoreactive somata localized to the anterior superior medial protocerebrum uniquely labeled by *tdc2-GAL4* (the ASM cluster; Fig. 1C). Yet they are not necessarily octopaminergic, as there are GAL4-positive neurons without OA-immunoreactivity in this cluster (Fig. 2G). We categorized these neurons into three types based on the repeatedly observed and distinct projection patterns (OA-ASM1-3; Fig. 13, Table 3). OA-ASM2 and OA-ASM3 differ only in the tract that crosses the midline, although the other characters are common, including the terminal areas. Since the fine projection pattern of these neurons remains ambiguous because of the faint labeling of individual ASM neurons, further classification of cell types might be possible. All the GAL4-expressing neurons in the ASM cluster send a process to the posterior protocerebrum where it branches out in a cell type-specific manner (Fig. 13).

OA-ASM1 has extensive ramifications in the ipsilateral side of the brain, i.e., throughout the posterior protocerebrum and the anterior superior lateral protocerebrum (Fig. 13C). From the posterior ramifications, a single branch emerges and bifurcates in the area dorsolateral to the esophagus foramen.

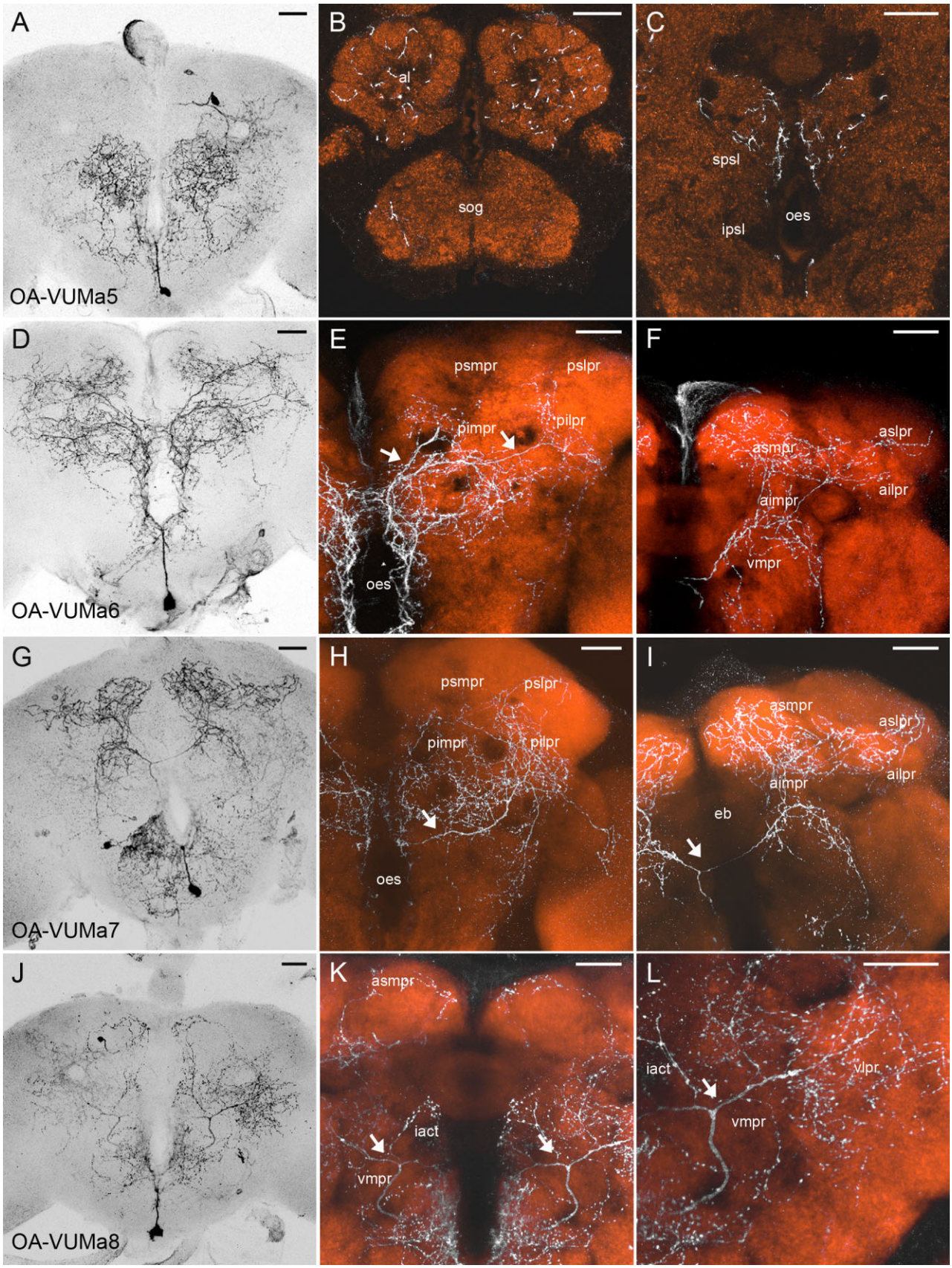


Figure 11

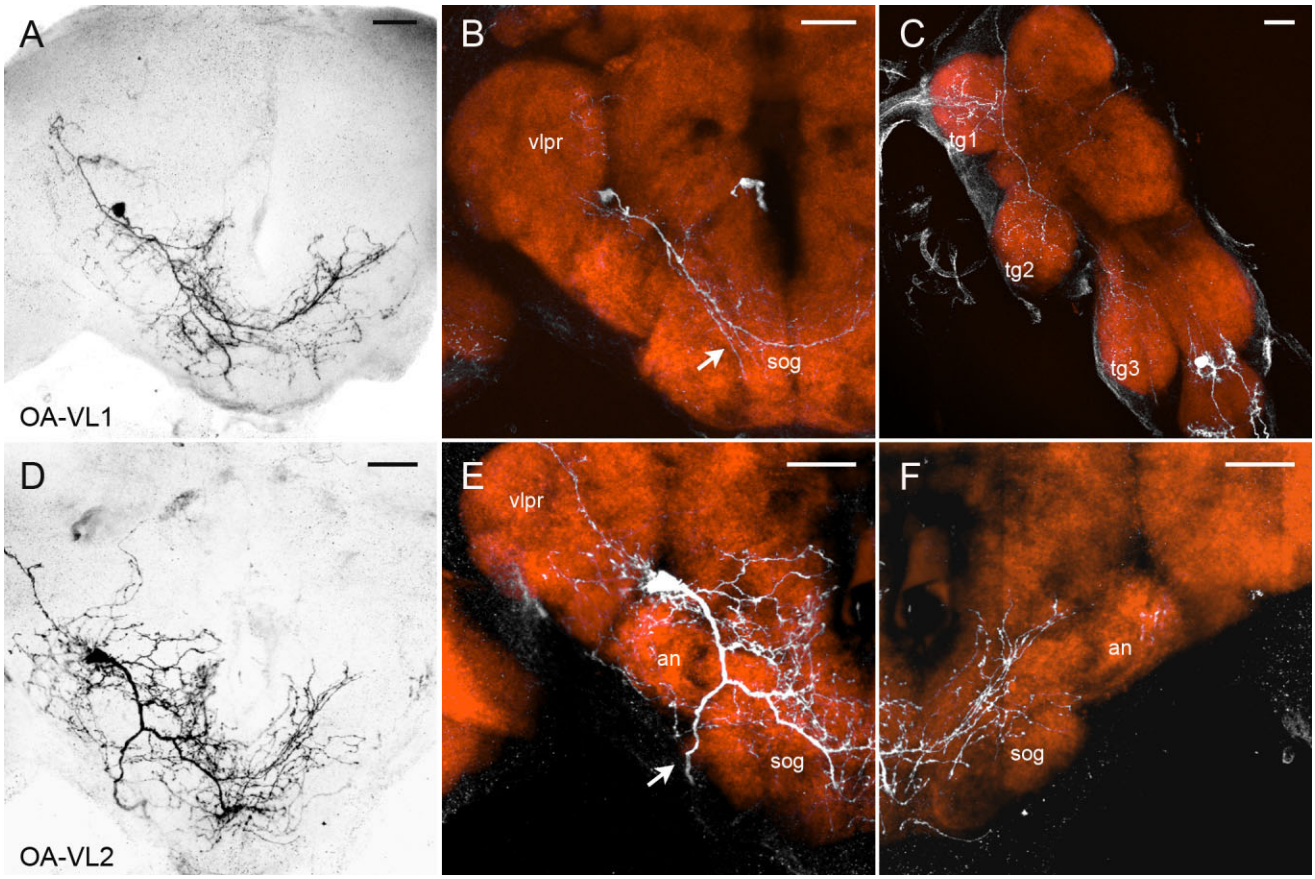


Figure 12.
Single-cell staining of VL neurons. The panels and the color scheme are organized as in Figure 6. **B:** OA-VL1 sends a process to the SOG (sog) where it crosses the midline. It ramifies in the ventrolateral protocerebrum (vlpr) and the subesophageal ganglion (sog). A Single process of OA-VL1 (arrow) projects through the posterior SOG to the cervical connectives. **C:** Innervations of OA-VL1 in the ipsilateral ventral nerve cord, i.e., the thoracic ganglia 1–3 (tg1-3). **E,F:** A neurite emerging from OA-VL2 crosses the midline in the subesophageal ganglion (sog). It ramifies in the ventrolateral protocerebrum (vlpr), the antennal nerves (an), and the subesophageal ganglion (sog). A single process of OA-VL2 (arrow) runs along the lateral margin of the subesophageal ganglion to the cervical connectives. Scale bars = 25 $\mu$m.

Figure 11.
Flp-out clones of ascending OA-VUM neurons underrepresented across all prepared samples. The panels and the color scheme are organized as in Figure 6. **A–C:** Varicose terminals of OA-VUMa5 are localized in the antennal lobes (al). C: Spiny ramifications of OA-VUMa5 extend around the esophagus foramen. **D–F:** OA-VUMa6 mainly innervates posterior protocerebrum with two laterally projecting branches (arrows) from the dorsal esophagus (oes). E: Ramification in the inferior (pimpr, pilpr), and the superior (psmpr, pslpr) protocerebrum. F: Innervations of OA-VUMa6 in the anterior protocerebrum (i.e., the ventromedial [vmpr], the inferior [aimpr, ailpr], and the superior [asmpr, aslpr] protocerebrum). **G–I:** Projection pattern of OA-VUMa7. H: Projected confocal stacks in the posterior region. A characteristic neurite (arrow) projects to the inferior lateral protocerebrum (pilpr). I: Projection of confocal stacks in the anterior region with a branch (arrow) bifurcating at the ventral to the ellipsoid body (eb). The emerging neurites ramify anterior in the inferior (aimpr, ailpr) and superior (asmpr, aslpr) protocerebrum. **J–L:** Innervation of OA-VUMa8. K,L: Neurites of OA-VUMa8 which bifurcate (arrows) in the ventromedial protocerebrum (vmpr), i.e., ventrolateral to the inner antennocerebral tract (iact). The emerging branches ramify in the ventrolateral protocerebrum (vlpr) and the anterior superior medial protocerebrum (asmpr), respectively. Scale bars = 25 $\mu$m.

One process projects to the ipsilateral optic lobe. The other one crosses the midline dorsal to the fan-shaped body and innervates the contralateral optic lobe (Fig. 13A). Both processes branch out in the inner medulla and the lobula of both optic lobes (Fig. 13D).

The primary neurite of OA-ASM2 bifurcates dorsolateral to the fan-shaped body (Fig. 13E,G). One process projects laterally and ramifies extensively in the ipsilateral posterior protocerebrum, i.e., around the pedunculus of the mushroom body (Fig. 13F). The other process bifurcates again above the fan-shaped body (Fig. 13G, arrows). The emerging branches run laterally to the midline. Then they project to the posterior where they turn toward the ipsilateral and contralateral inferior protocerebra, respectively. The contralateral branch crosses the midline dorsal of the fan-shaped body (Fig. 13G,H, arrows). Each of the two branches ramifies in the inferior and in the ventrolateral protocerebra.

In the case of OA-ASM3 (Fig. 13I–L), the bifurcation of the primary neurite is also located dorsolateral to the fan-shaped body (Fig. 13I). One process runs laterally, targeting the superior protocerebrum (Fig. 13J). The other process crosses

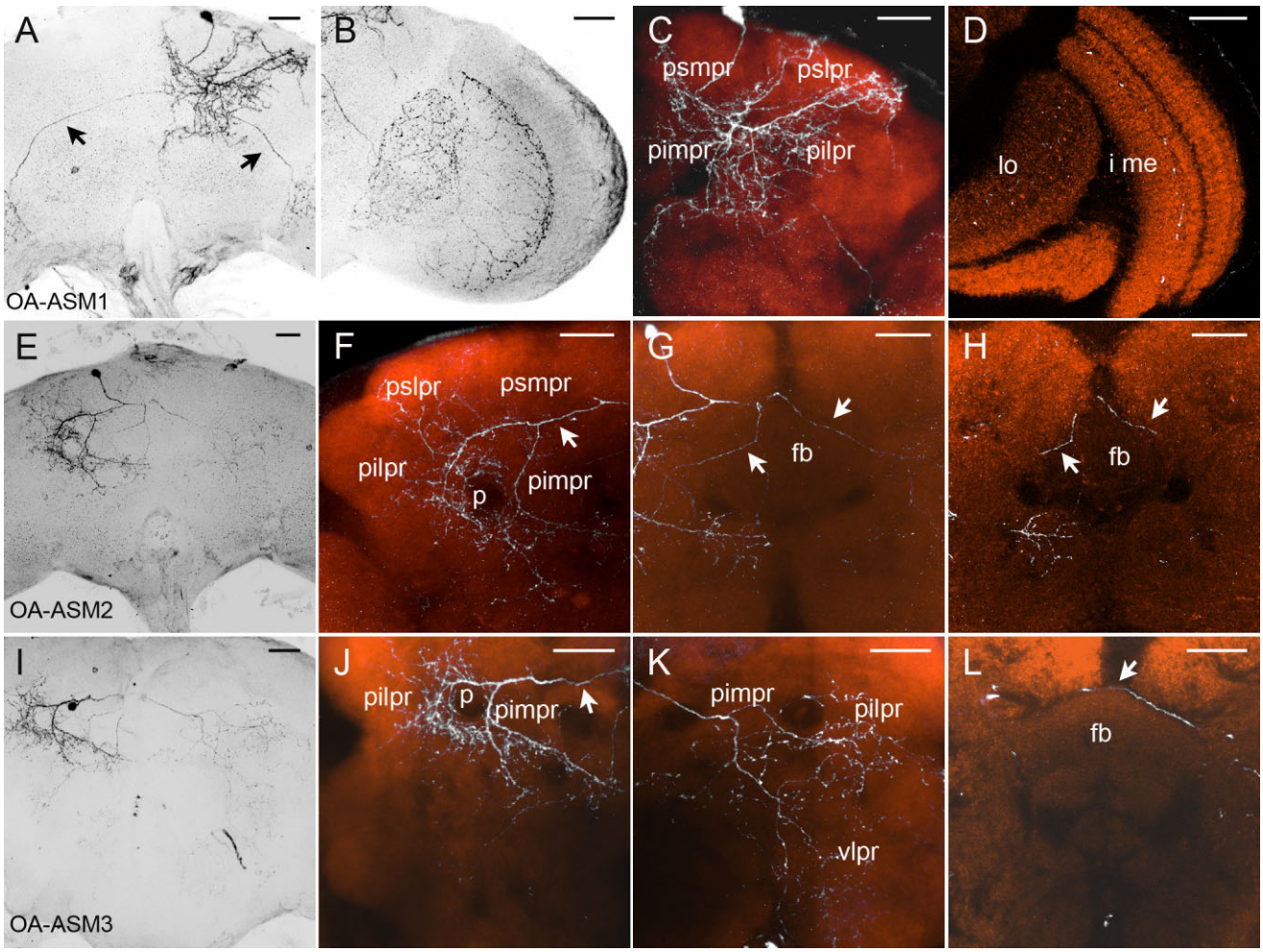


Figure 13.
Single-cell staining of OA-ASM neurons. The panels and the color scheme are organized as in Figure 6. **A,B:** From posterior ramifications of OA-ASM1 emerge two neurites (arrows in A) targeting the ipsilateral and the contralateral optic lobe, respectively. **C:** OA-ASM1 ramifies extensively in the ipsilateral posterior protocerebra (psmpr, pslpr, pimpr, pilpr). **D:** In the otpic lobes OA-ASM1 innervates the inner medulla (i me) and the lobula (lo). **F:** OA-ASM2 bifurcates dorsolateral to the fan-shaped body. One emerging process (arrow) projects to the lateral. It ramifies extensively in the ipsilateral posterior protocerebra (psmpr, pslpr, pimpr, pilpr), i.e., around the pedunculus (p). **G,H:** The other process bifurcates again. The emerging branches (arrows) run along the midline to the posterior where they turn to the lateral. **J:** OA-ASM3 bifurcates dorsolateral to the fan-shaped body. One process (arrow) runs to the lateral to target the inferior protocerebrum (pimpr, pilpr). **J,K:** OA-ASM3 ramifies in the posterior protocerebra (J, pimpr, pilpr), and the ventrolateral protocerebrum (K, vlpr). Especially the ipsilateral protocerebra, i.e., the region around the pedunculus, exhibits extensive innervations (J). **L:** OA-ASM3 crosses the midline dorsal of the fan-shaped body (arrow). Scale bars = 25 $\mu$m.

the midline dorsal to the fan-shaped body (Fig. 13L, arrow). These processes give rise to complicated ramifications in the posterior and ventrolateral protocerebra as well as the SOG (Fig. 13J,K). Especially the ipsilateral protocerebrum, i.e., the region around the peduncle, exhibits dense innervation.

## DISCUSSION

Taking advantage of genetic methods, the present study described the morphology of candidate octopaminergic neurons in the *Drosophila* brain. Application of the Flp-out technique (Wong et al., 2002) enabled comprehensive visualization of the morphology of individual octopaminergic neurons. This first systematic identification revealed a common cellular ar-

Figure 14.
Two examples of stereotypy. Innervation patterns of OA-AL2i1 (A–L) and OA-VPM1 (M–U) in three different samples. The left-most column depict projections of confocal stacks illustrating the overall projection patterns of different samples. Right columns depict ramifications of each sample monitored by mCD8::GFP (white) in the neuropil staining (orange). **A–L:** Each sample of OA-AL2i1 exhibits a similar innervation pattern in the inferior and superior posterior slope (ipsl and spsl in B,F,J), the protocerebral bridge (pb in C,G,K), and the optic lobe (D,H,L; I me: inner medulla, lo: lobula, lop: lobula plate). The black arrow in I indicates a simultaneously labeled different cell. **M–U:** Each sample of OA-VPM1 exhibits a similar innervation pattern in the ventromedial protocerebrum (vmpr) and the SOG (N,Q,T). In each sample a characteristic secondary neurite was identified, which branches off ventromedial to the esophagus (oes) into te ipsilateral brain hemisphere (arrows, O,R,U). Scale bars = 25 $\mu$m.

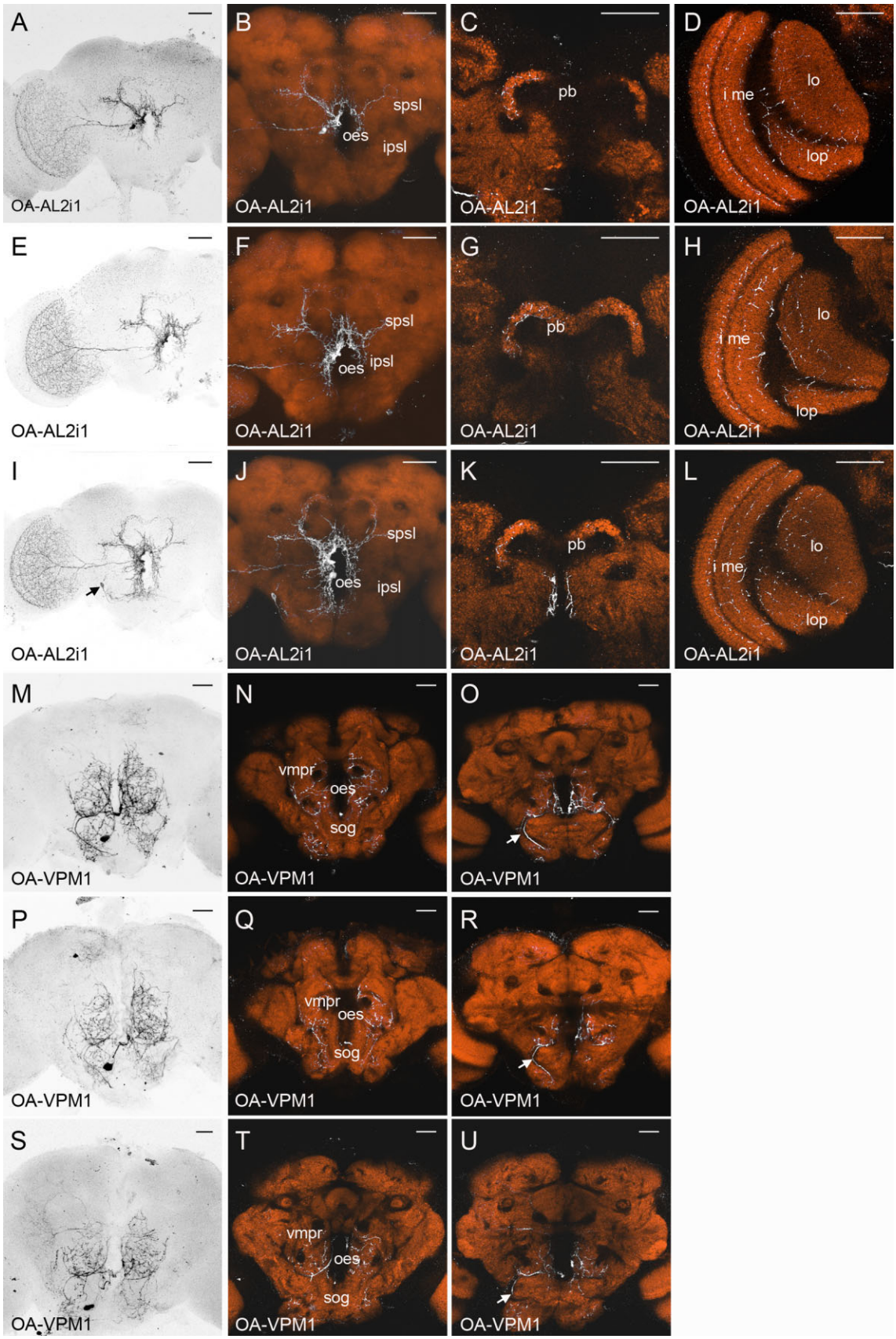


Figure 14

chitecture of octopaminergic neurons: most of them receive main inputs in one specific brain area, i.e., the posterior slope, and each neuron typically targets several defined neuropil regions in the brain. The cells differ from each other mainly in the combination of their target regions. Since OA regulates a large repertoire of behaviors, this anatomical map may help identify the underlying neural circuit for each behavioral modulation mediated by OA.

## Large-scale identification of individual octopaminergic neurons

The random mosaic labeling in *NP7088* and *tdc2-GAL4* allowed us to visualize most of the individual GAL4-expressing neurons. Based on the double labeling of the GAL4 lines with the anti-OA antibody, we assume that 27 GAL4-expressing neurons distributed in clusters VM, AL2, VL, and ASM are octopaminergic. Among the 16 different cell types identified in the VM cluster, 11 types are OA-VUM neurons and the other five types are OA-VPM neurons. Since OA-VPM neurons are paired and some of the OA-VUM neurons seem to be duplicated (data not shown), this study identified most, if not all, of the 27 neurons in the VM cluster.

The projection patterns of the OA-immunoreactive and GAL4-expressing neurons were mostly consistent with a previous report on the cellular distribution of OA (Sinakevitch and Strausfeld, 2006). Yet it remains to be confirmed whether the cells in cluster ASM and OA-AL2b2 are indeed octopaminergic (Figs. 1C, 2G, 7D). Although we reproducibly found immunolabeling in this cluster (Fig. 2G), these cells have not been reported to be OA-immunoreactive (Monastirioti et al., 1995; Sinakevitch and Strausfeld, 2006). Although the crossreactivity of the anti-OA antibody to TA was controlled (Suppl. Figs. 2, 3), these neurons might be tyraminergic without producing OA, as proposed in the *Drosophila* larva (Nagaya et al., 2002). Despite the technical difficulty of the transmitter staining, a comparison of the expression patterns of Tdc2 and T$\beta$h, an enzyme specifically required for OA, but not TA, synthesis, would reveal the existence of such tyraminergic neurons.

It is important to mention that both GAL4 drivers we employed in this study do not cover all the octopaminergic neurons labeled with the anti-OA antibody (Fig. 2). Since those octopaminergic cells not described in this study may play important roles in OA-mediated behavioral modulation (e.g., the neurons projecting to the ellipsoid body), completing the map by identifying the morphology of those neurons is of particular importance.

## Anatomical hallmarks of octopaminergic neurons

Judged by the distribution of presynaptic and postsynaptic marker proteins, the majority of octopaminergic neurons appear to be highly polarized (Figs. 4, 5), i.e., main input and output regions are clearly separated. Varicose terminals, which are colocalized with the presynaptic marker, are distributed throughout the brain. In contrast, spiny arbors of neurons of clusters VM and AL2 are localized in the posterior slope, where the postsynaptic marker Rdl-HA is highly concentrated (Fig. 5). Consistently, OA immunolabeling was less intense in this region compared to other presynaptic regions (data not shown; Monastirioti et al., 1995; Sinakevitch and Strausfeld, 2006). This polarized architecture suggests that these neurons are designed to collect synaptic inputs in the posterior slope and to modulate an array of targets by giving outputs in distinct neuropils in the brain. Afferent neurons that are presynaptic to the octopaminergic neurons remain to be identified. The characteristic polarity may open a possibility to identify the entire neural circuits underlying the neuromodulation by OA.

The single cell morphology of these neurons revealed that each cell type stereotypically innervates a distinct combination of brain regions (Figs. 14, 15). For instance, the mushroom bodies and the optic lobes are innervated by different groups of neurons. The cells of each group target distinct subregions within those neuropils (Fig. 15). For example, OA-VPM3 terminates in the fan-shaped body and the nodulli of the central complex, whereas another neuron, OA-AL2i1, projects only to the protocerebral bridge. Similarly, the six types of the descending neurons exhibit distinct projection patterns (Fig. 15). These strongly suggest that octopaminergic neurons are organized in a combinatorial manner: Each individual neuron seems to be a component of specific neural circuits. Thus, each type of octopaminergic neurons could serve as a "module" that could selectively modulate the function of a respective area of the brain, (Fig. 15). The stereotypy of these neurons might be confirmed by aligning the same type of octopaminergic neurons in different brains using computer algorithms (Jenett et al., 2006; Jefferis et al., 2007; Datta et al., 2008). However, such programs available at the current time produced large errors in aligning single cells in the entire brains of different samples (data not shown). Thus, we here present our microscopic data without such standardization (Fig. 14).

## Comparative and functional perspectives

The overall organization and function of the brain are conserved between different insect species. Interestingly, some anatomical traits of octopaminergic neurons in *Drosophila* are extremely similar to those of other species, suggesting their conserved functions.

One of the morphological hallmarks of octopaminergic neurons in *Drosophila* is the highly enriched dendritic region in the posterior slope (Figs. 5, 15). The studies on single cell morphology of octopaminergic neurons in the honeybee and locust showed that several DUM or VUM neurons in the SOG of the locust or honeybee terminate in the corresponding region (Bräunig, 1991; Bräunig and Burrows, 2004; Schröter et al., 2007). However, partially due to the lack of a transgenic marker, such centralized postsynapses have been less obvious in these insects. This interspecies difference might be due to the fact that each neuromere is clearly segregated in these insects, whereas the neuromeres in the *Drosophila* SPG and SOG are fused and therefore condensed. Further investigation of the spatial relationship between the dendrites of different octopaminergic neurons might illuminate an internal structure within the enriched dendritic regions.

Antibody labeling of OA has visualized paired cells lateral to the midline neurons in various insect species (Stevenson and Spörhase-Eichmann, 1995; Sinakevitch et al., 2005). Compared to the other insects such as honeybees, crickets, locusts, and cockroaches, *Drosophila* seems to have more paired octopaminergic neurons in the SOG (Stevenson and Spörhase-Eichmann, 1995; Sinakevitch et al., 2005). The morphology of these paired median neurons has been unknown. The single-cell analysis in this study, for the first time, revealed the projection pattern of each subesophageal VPM

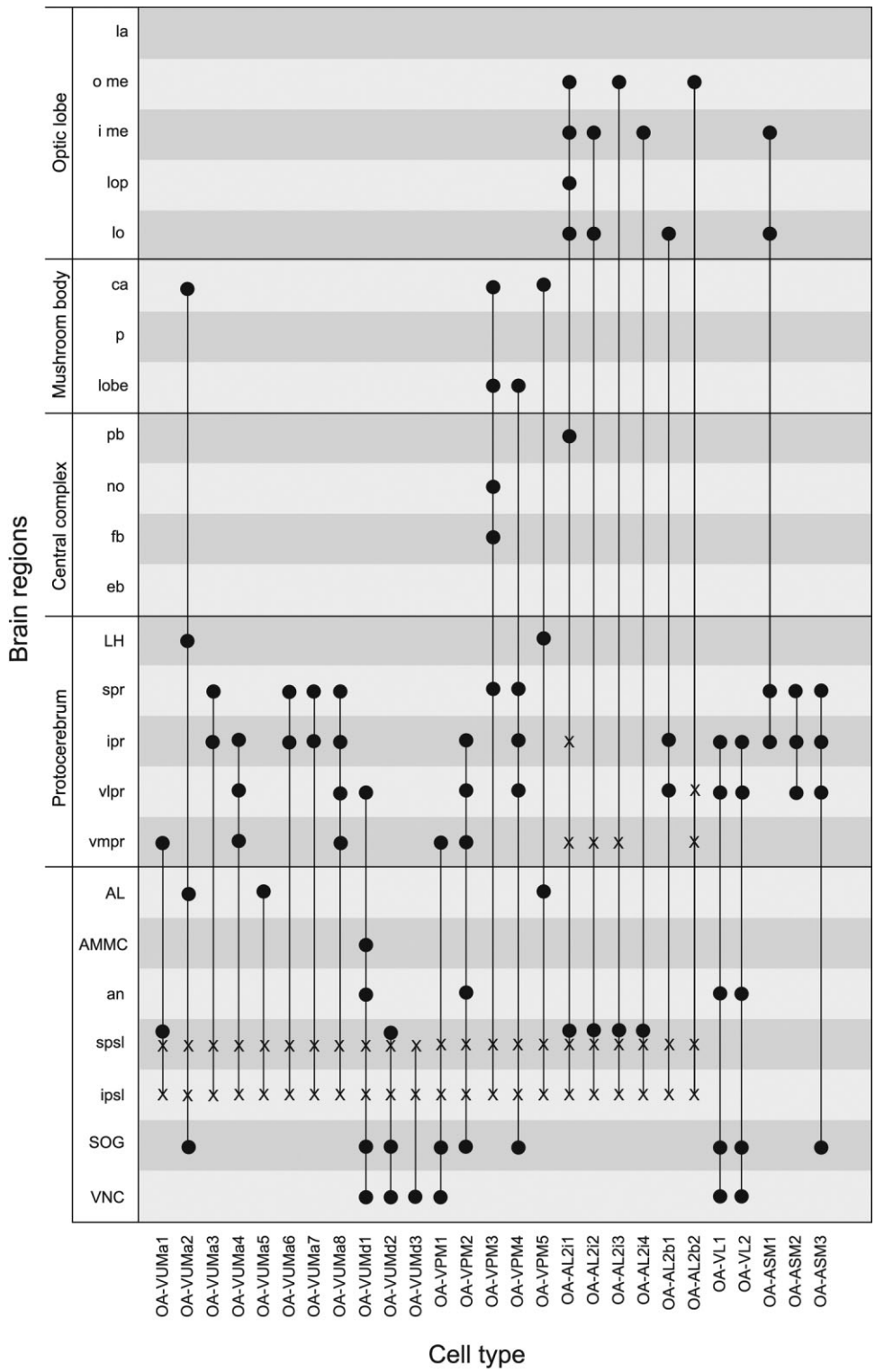


Figure 15.
Schematic diagram of the innervation areas of all individual cell types analyzed in this study. Dots represent neuropils containing varicose nerve terminals of each individual cell type. Regions with spiny ramifications are labeled with X. The target regions of individual cell types are connected by a line. Each neuropil is innervated by a distinct set of neurons, suggesting a combinatorial organization of octopaminergic neurons. VNC, ventral nerve cord; ipsl, inferior posterior slope; spsl, superior posterior slope; SOG, subesophageal ganglion; an, antennal nerve; AMMC, antennal mechanosensory and motor center; AL, antennal lobe; vmpr, ventromedial protocerebrum; vlpr, ventrolateral protocerebrum; ipr, inferior protocerebrum; spr, superior protocerebrum; LH, lateral horn; fb, fan-shaped body; no, noduli; pb, protocerebral bridge; lobe, mushroom body lobes; ca, calyx; lo, lobula; lop, lobula plate; i me, inner medulla; o me, outer medulla; la, lamina.

neuron (Fig. 8). As in OA-VUM neurons, OA-VPM neurons, yet asymmetrically, exhibit extensive projections to distinct brain regions with similar neuronal polarity.

Importantly, our analysis identified a pair of OA-VPM neurons that might be a counterpart of an unpaired median neuron in another insect. We found that OA-VPM3 innervates the fan-shaped body of the central complex, the calyx of the mushroom body, and parts of the superior protocerebrum (Fig. 8I–L). These target brain regions match those innervated by a single subesophageal DUM neuron in the locust (SA1) (Bräunig, 1991). SA1 has mirror-symmetric processes and terminate in parts of the central complex, various protocerebral regions, and the calyces. Based on the anatomical homology of the octopaminergic neurons between these two species we speculate that both neurons could fulfill similar functions. The replacement of unpaired with paired neurons might be the reason for a larger number of OA-VPM neurons in *Drosophila*.

In other insect species, subesophageal VUM/DUM neurons potentially modulate various sensory afferents and behaviors by innervating sensory nerves (Long and Murdock, 1983; Bräunig and Pflüger, 2001; Scheiner et al., 2002). Consistently, efferent octopaminergic neurons in these insects are found to project through the sensory nerves, such as the antennal nerves (Bräunig, 1991; Bräunig and Pflüger, 2001; Schröter et al., 2007). The neurons in the VM and AL2 clusters in *Drosophila* extensively innervate the terminal areas of sensory neurons including the optic lobes, the antennal mechanosensory and motor centers, the antennal lobes, and the SOG. Therefore, primary sensory information might be modulated directly by OA. Although we identified no efferent octopaminergic neuron, we assume that this might be due to a technical reason. Because our whole-mount preparation usually cuts the sensory nerves at the level close to the brain, single efferent fibers would not be detected.

The neurons of cluster AL2 innervate the medulla, lobula, and lobula plate, but not lamina (Figs. 6, 7). This cluster consists of ipsilaterally and bilaterally projecting neurons (OA-AL2i and OA-AL2b, respectively). Importantly, they share striking structural similarity to the neurons PM4 and PM5 in the locust (Stern et al., 1995; Stern, 1999). They are shown to be involved in dishabituating the response of the descending contralateral movement detector. Given their homologous cellular architecture, OA-AL2i neurons in *Drosophila* might modulate visual information in a similar manner. It should be important to clarify whether these neurons directly synapse onto sensory neurons. Because of the lack of AL2 cluster neurons and OA-immunoreactivity in the lamina (Sinakevitch and Strausfeld, 2006) (data not shown), only the inner photoreceptors (i.e., R7 and R8 cells of the ommatidia) are eligible for the direct sensory targets in the optic lobes.

Our large-scale analysis identified six different descending octopaminergic neurons: three types of VUM (OA-VUMd) neurons, one type of OA-VPM neurons, and two types of OA-VL neurons. Except for OA-VUMd3, they all have ascending processes in the brain as well as descending secondary neurites into the cervical connectives (Figs. 8, 12, 13, 15). Interestingly, all three types of OA-VUMd neurons we found belong to the posteriormost subcluster, i.e., VMlb (Fig. 10). This morphological hallmark is consistent with the organization in the locust. The majority of the descending subesophageal DUM neurons in the locust belong to the posterior subcluster (Bräunig and Burrows, 2004). These descending octopaminergic neurons might regulate motor control in the thoracic ganglia, since OA is reported to stimulate certain motor behaviors, such as locomotion and grooming (Yellman et al., 1997).

In appetitive olfactory learning in the honeybee, the stimulation of the identified octopaminergic neuron VUMmx1 was shown to replace sugar reward (Hammer, 1993). VUMmx1 bilaterally innervates the antennal lobes, the calyces of the mushroom bodies, and the lateral horns in the bee brain. We also found a VUM neuron in *Drosophila* (OA-VUMa2) that project to the same brain structures. Since OA has a similar function in olfactory learning of *Drosophila* (Schwaerzel et al., 2003; Schroll et al., 2006), the role of OA-VUMa2 in reward processing can now be studied.

In summary, our comprehensive anatomical analysis of *Drosophila* octopaminergic neurons revealed a strong overall similarity to the organization in other insect species. The conserved architecture implies importance of the development of octopaminergic neurons for their functions. In addition, *Drosophila melanogaster* will serve as a genetically tractable model system to study functions, development, and evolution of octopaminergic neurons.

## ACKNOWLEDGMENTS

We thank K. Grübel and B. Mühlbauer for excellent technical assistance; N.K. Tanaka for the initial screening of the GAL4 drivers; Y. Aso, B. Gerber, M. Heisenberg, F. Leiss, C. Schnaitmann, and G. Tavosanis for discussion and critical reading of the article. H.T. and S.B. received Research Fellowship from Japan Society for the Promotion of Science, Long-Term Fellowship form Human Frontier Science Program, and doctoral fellowship from Boehringer-Ingelheim Fonds.

## LITERATURE CITED

Adamo SA, Linn CE, Hoy RR. 1995. The role of neurohormonal octopamine during 'fight or flight' behaviour in the field cricket Gryllus bimaculatus. J Exp Biol 198(Pt 8):1691–1700.

Bräunig P. 1991. Suboesophageal DUM neurons innervate the principal neuropiles of the locust brain. Philos Trans R Soc Lond B Biol Sci 332:221–240.

Bräunig P, Burrows M. 2004. Projection patterns of posterior dorsal unpaired median neurons of the locust suboesophageal ganglion. J Comp Neurol 478:164–175.

Bräunig P, Pflüger H-J. 2001. The unpaired median neurons of insects. Adv Insect Physiol 28:185–266.

Certel SJ, Savella MG, Schlegel DC, Kravitz EA. 2007. Modulation of *Drosophila* male behavioral choice. Proc Natl Acad Sci U S A 104: 4706–4711.

Cole SH, Carney GE, McClung CA, Willard SS, Taylor BJ, Hirsh J. 2005. Two functional but non-complementing Drosophila tyrosine decarboxylase genes: distinct roles for neural tyramine and octopamine in female fertility. J Biol Chem 280:14948–14955.

Dacks AM, Christensen TA, Agricola HJ, Wollweber L, Hildebrand JG. 2005. Octopamine-immunoreactive neurons in the brain and suboesophageal ganglion of the hawkmoth *Manduca sexta*. J Comp Neurol 488:255–268.

Datta SR, Vasconcelos ML, Ruta V, Luo S, Wong A, Demir E, Flores J, Balonze K, Dickson BJ, Axel R. 2008. The *Drosophila* pheromone cVA activates a sexually dimorphic neural circuit. Nature 452:473–477.

Downer RGH, Orr GL, Gole JWD, Orchard I. 1984. The role of octopamine and cyclic AMP in regulating hormone release from corpora cardiaca of the American cockroach. J Insect Physiol 30:457–462.

Evans PD, O'Shea M. 1977. An octopaminergic neurone modulates neuromuscular transmission in the locust. Nature 270:257–259.

Farooqui T. 2007. Octopamine-mediated neuromodulation of insect senses. Neurochem Res 32:1511–1529.

Geffard M, Seguela P, Heinrich-Rock AM. 1984. Antisera against catecholamines: specificity studies and physicochemical data for anti-dopamine and anti-p-tyramine antibodies. Mol Immunol 21:515–522.

Godenschwege TA, Reisch D, Diegelmann S, Eberle K, Funk N, Heisenberg M, Hoppe V, Hoppe J, Klagges BR, Martin JR, Nikitina EA, Putz G, Reifegerste R, Reisch N, Rister J, Schaupp M, Scholz H, Schwarzel M, Werner U, Zars TD, Buchner S, Buchner E. 2004. Flies lacking all synapsins are unexpectedly healthy but are impaired in complex behaviour. Eur J Neurosci 20:611–622.

Hammer M. 1993. An identified neuron mediates the unconditioned stimulus in associative olfactory learning in honeybees. Nature 366:59–63.

Hayashi S, Ito K, Sado Y, Taniguchi M, Akimoto A, Takeuchi H, Aigaki T, Matsuzaki F, Nakagoshi H, Tanimura T, Ueda R, Uemura T, Yoshihara M, Goto S. 2002. GETDB, a database compiling expression patterns and molecular locations of a collection of Gal4 enhancer traps. Genesis 34:58–61.

Hoyer SC, Eckart A, Herrel A, Zars T, Fischer SA, Hardie SL, Heisenberg M. 2008. Octopamine in male aggression of *Drosophila*. Curr Biol 18:159–167.

Ito K, Okada R, Tanaka NK, Awasaki T. 2003. Cautionary observations on preparing and interpreting brain images using molecular biology-based staining techniques. Microsc Res Tech 62:170–186.

Jefferis GS, Potter CJ, Chan AM, Marin EC, Rohlfing T, Maurer CR Jr, Luo L. 2007. Comprehensive maps of *Drosophila* higher olfactory centers: spatially segregated fruit and pheromone representation. Cell 128: 1187–1203.

Jenett A, Schindelin JE, Heisenberg M. 2006. The Virtual Insect Brain protocol: creating and comparing standardized neuroanatomy. BMC Bioinformatics 7:544.

Klagges BR, Heimbeck G, Godenschwege TA, Hofbauer A, Pflugfelder GO, Reifegerste R, Reisch D, Schaupp M, Buchner S, Buchner E. 1996. Invertebrate synapsins: a single gene codes for several isoforms in *Drosophila*. J Neurosci 16:3154–3165.

Konings PN, Vullings HG, Geffard M, Buijs RM, Diederen JH, Jansen WF. 1988. Immunocytochemical demonstration of octopamine-immunoreactive cells in the nervous system of *Locusta migratoria* and *Schistocerca gregaria*. Cell Tissue Res 251:371–379.

Kreissl S, Eichmuller S, Bicker G, Rapus J, Eckert M. 1994. Octopamine-like immunoreactivity in the brain and suboesophageal ganglion of the honeybee. J Comp Neurol 348:583–595.

Lee T, Luo L. 1999. Mosaic analysis with a repressible cell marker for studies of gene function in neuronal morphogenesis. Neuron 22:451–461.

Long TF, Murdock LL. 1983. Stimulation of blowfly feeding behavior by octopaminergic drugs. Proc Natl Acad Sci U S A 80:4159–4163.

Mercer AR, Menzel R. 1982. The effects of biogenic amines on conditioned and unconditioned responses to olfactory stimuli in the honeybee *Apis mellifera*. J Comp Physiol [A] 145:363–368.

Monastirioti M. 2003. Distinct octopamine cell population residing in the CNS abdominal ganglion controls ovulation in *Drosophila melanogaster*. Dev Biol 264:38–49.

Monastirioti M, Gorczyca M, Rapus J, Eckert M, White K, Budnik V. 1995. Octopamine immunoreactivity in the fruit fly *Drosophila melanogaster*. J Comp Neurol 356:275–287.

Monastirioti M, Linn CE Jr, White K. 1996. Characterization of *Drosophila* tyramine beta-hydroxylase gene and isolation of mutant flies lacking octopamine. J Neurosci 16:3900–3911.

Nagaya Y, Kutsukake M, Chigusa SI, Komatsu A. 2002. A trace amine, tyramine, functions as a neuromodulator in *Drosophila melanogaster*. Neurosci Lett 329:324–328.

Otsuna H, Ito K. 2006. Systematic analysis of the visual projection neurons of *Drosophila melanogaster*. I. Lobula-specific pathways. J Comp Neurol 497:928–958.

Ramirez J-M, Orchard IAN. 1990. Octopaminergic modulation of the forewing stretch receptor in the locust *Locusta migratoria*. J Exp Biol 149:255–279.

Robinson IM, Ranjan R, Schwarz TL. 2002. Synaptotagmins I and IV promote transmitter release independently of Ca(2+) binding in the C(2)A domain. Nature 418:336–340.

Roeder T. 1999. Octopamine in invertebrates. Prog Neurobiol 59:533–561.

Roeder T. 2005. Tyramine and octopamine: ruling behavior and metabolism. Annu Rev Entomol 50:447–477.

Sanchez-Soriano N, Bottenberg W, Fiala A, Haessler U, Kerassoviti A, Knust E, Lohr R, Prokop A. 2005. Are dendrites in *Drosophila* homologous to vertebrate dendrites? Dev Biol 288:126–138.

Scheiner R, Pluckhahn S, Oney B, Blenau W, Erber J. 2002. Behavioural pharmacology of octopamine, tyramine and dopamine in honey bees. Behav Brain Res 136:545–553.

Scholz H, Ramond J, Singh CM, Heberlein U. 2000. Functional ethanol tolerance in *Drosophila*. Neuron 28:261–271.

Schroll C, Riemensperger T, Bucher D, Ehmer J, Völler T, Erbguth K, Gerber B, Hendel T, Nagel G, Buchner E, Fiala A. 2006. Light-induced activation of distinct modulatory neurons triggers appetitive or aversive learning in *Drosophila* larvae. Curr Biol 16:1741–1747.

Schröter U, Malun D, Menzel R. 2007. Innervation pattern of suboesophageal ventral unpaired median neurones in the honeybee brain. Cell Tissue Res 327:647–667.

Schwaerzel M, Monastirioti M, Scholz H, Friggi-Grelin F, Birman S, Heisenberg M. 2003. Dopamine and octopamine differentiate between aversive and appetitive olfactory memories in *Drosophila*. J Neurosci 23: 10495–10502.

Sinakevitch I, Strausfeld NJ. 2006. Comparison of octopamine-like immunoreactivity in the brains of the fruit fly and blow fly. J Comp Neurol 494:460–475.

Sinakevitch IG, Geffard M, Pelhate M, Lapied B. 1995. Octopaminergic dorsal unpaired median (DUM) neurones innervating the colleterial glands of the female cockroach *Periplaneta americana*. J Exp Biol 198(Pt 7):1539–1544.

Sinakevitch I, Niwa M, Strausfeld NJ. 2005. Octopamine-like immunoreactivity in the honey bee and cockroach: comparable organization in the brain and suboesophageal ganglion. J Comp Neurol 488:233–254.

Spörhase-Eichmann U, Vullings HG, Buijs RM, Horner M, Schurmann FW. 1992. Octopamine-immunoreactive neurons in the central nervous system of the cricket, Gryllus bimaculatus. Cell Tissue Res 268:287–304.

Stern M. 1999. Octopamine in the locust brain: cellular distribution and functional significance in an arousal mechanism. Microsc Res Tech 45:135–141.

Stern M, Thompson KSJ, Zhou P, Watson DG, Midgley JM, Gewecke M, Bacon JP. 1995. Octopaminergic neurons in the locust brain: morphological, biochemical and electrophysiological characterisation of potential modulators of the visual system. J Comp Physiol [A] 177:611–625.

Stevenson PA, Spörhase-Eichmann U. 1995. Localization of octopaminergic neurones in insects. Comp Biochem Physiol A Physiol 110:203–215.

Stevenson PA, Hofmann HA, Schoch K, Schildberger K. 2000. The fight and flight responses of crickets depleted of biogenic amines. J Neurobiol 43:107–120.

Tanaka NK, Tanimoto H, Ito K. 2008. Neuronal assemblies of the *Drosophila* mushroom body. J Comp Neurol 508:711–755.

Van Dyke MW, Nelson LD, Weilbaecher RG, Mehta DV. 2004. Stm1p, a G4 quadruplex and purine motif triplex nucleic acid-binding protein, interacts with ribosomes and subtelomeric Y' DNA in *Saccharomyces cerevisiae*. J Biol Chem 279:24323–24333.

Vergoz V, Roussel E, Sandoz JC, Giurfa M. 2007. Aversive learning in honeybees revealed by the olfactory conditioning of the sting extension reflex. PLoS ONE 2:e288.

Wong AM, Wang JW, Axel R. 2002. Spatial representation of the glomerular map in the *Drosophila* protocerebrum. Cell 109:229–241.

Yellman C, Tao H, He B, Hirsh J. 1997. Conserved and sexually dimorphic behavioral responses to biogenic amines in decapitated *Drosophila*. Proc Natl Acad Sci U S A 94:4131–4136.

Zhou C, Rao Y. 2008. A subset of octopaminergic neurons are important for Drosophila aggression. Nat Neurosci (in press).